

Measuring ultrashort laser pulses in the time-frequency domain using frequency-resolved optical gating

Rick Trebino, Kenneth W. DeLong, David N. Fittinghoff, John N. Sweetser, Marco A. Krumbügel, and Bruce A. Richman
Combustion Research Facility, Sandia National Labs, Livermore, California 94550

Daniel J. Kane
Southwest Sciences, Incorporated, Suite E-11, 1570 Pacheco Street, Santa Fe, New Mexico 87501

(Received 9 December 1996; accepted for publication 9 May 1997)

We summarize the problem of measuring an ultrashort laser pulse and describe in detail a technique that completely characterizes a pulse in time: frequency-resolved optical gating. Emphasis is placed on the choice of experimental beam geometry and the implementation of the iterative phase-retrieval algorithm that together yield an accurate measurement of the pulse time-dependent intensity and phase over a wide range of circumstances. We compare several commonly used beam geometries, displaying sample traces for each and showing where each is appropriate, and we give a detailed description of the pulse-retrieval algorithm for each of these cases. © 1997 American Institute of Physics. [S0034-6748(97)00209-8]

I. THE PROBLEM OF MEASURING AN ULTRASHORT LASER PULSE

The past decade has seen tremendous progress in the development of lasers that emit ultrashort pulses.¹⁻⁴ Light pulses are approaching durations of a single optical cycle—one to two femtoseconds (10^{-15} s) for visible and near-IR wavelengths. And, in addition, the use of ultrashort pulses for both fundamental studies and applications is increasing rapidly.⁵⁻⁸

As these pulses shrink in length and grow in utility, the ability to measure them becomes increasingly important. There are several reasons for this. First, precise knowledge of the pulse properties is necessary for verifying theoretical models of pulse creation.^{9,10} Second, in order to make even shorter pulses, it is necessary to understand the distortions that limit the length of currently available pulses.^{9,10} Third, in experiments using these pulses, it is always important to know at least the pulse length in order to determine the temporal resolution of a given experiment. Moreover, in many experiments—studies of molecular vibrations, for example—additional details of the pulse's structure play an important role in determining the outcome of the experiment. Of particular importance is the variation of frequency during the pulse, known as "chirp." For example, chirped pulses can cause much greater molecular photodissociation than unchirped pulses.⁶ Fourth, a new class of material-characterization techniques is now evolving that depends heavily on the ability to precisely characterize an ultrashort pulse experimentally. More detailed material information can be discerned by fully characterizing the input and output pulses in such methods.^{11,12} Finally, numerous applications have emerged for shaped ultrashort pulses,^{13,14} and, of course, it is necessary to be able to measure the shape of the pulse used in these measurements.

Fortunately, in the past five years, remarkable progress

has occurred in the development of techniques for the measurement of ultrashort laser pulses. It is now routine to completely characterize the time dependence of these pulses in the laboratory.¹⁵⁻²⁰ With the most commonly used new pulse-measurement method, frequency-resolved optical gating, (FROG),^{16-18,21-34} it is now possible to measure pulses over a wide range of wavelengths, pulse lengths, and complexities and to do so in a manner that is general, robust, accurate, and rigorous. Single-shot measurement is straightforward.^{21,24,31} FROG measurements are insensitive to noise.^{28,35} Feedback regarding the quality of the data virtually eliminates the possibility that systematic error could cause one pulse to mimic another.^{23,32,34} Indeed, internal consistency checks in FROG even allow the correction of a trace for many types of systematic error, even when the source(s) of the error is unknown.³⁴ Complex apparatus is not necessary; FROG simply involves spectrally resolving the signal beam of an autocorrelation measurement. As most ultrafast laboratories already possess an autocorrelator and spectrometer for pulse measurement, complete pulse measurement using FROG requires no new apparatus. Finally, it is also possible to measure very weak pulses: combining FROG with spectral interferometry allows full characterization of a pulse train containing less than one photon per pulse on average.¹⁸

What does full characterization mean? The pulse is defined by its electric field as a function of time, $E(t)$. For the sake of simplicity, we treat the field as linearly polarized and therefore consider only the scalar component of it. We also assume that the pulse separates into the product of spatial and temporal factors, and we neglect the spatial factor. (We will discuss the spatiotemporal measurement of a pulse later.) The time-dependent component of the pulse can be written:

$$E(t) = \text{Re}\{\sqrt{I(t)} \exp(i\omega_0 t - i\varphi(t))\}, \quad (1)$$

where $I(t)$ and $\varphi(t)$ are the time-dependent intensity and phase of the pulse, and ω_0 is a carrier frequency. The time-dependent phase contains the frequency versus time information, and the pulse instantaneous frequency, $\omega(t)$, is given by

$$\omega(t) = \omega_0 - \frac{d\varphi}{dt}. \quad (2)$$

Thus, a constant-phase pulse experiences no frequency variation in time. Linear variation of φ in time is simply a frequency shift. But quadratic variation of φ with time represents a linear ramp of frequency versus time. Pulses with increasing frequency versus time are said to be “positively chirped,” and pulses with decreasing frequency versus time are said to be “negatively chirped.” When the phase distortion is simply quadratic, the chirp is said to be linear. Higher-order terms imply nonlinear chirp.

The pulse field can equally well be written in the frequency domain (neglecting the negative-frequency term):

$$\tilde{E}(\omega) = \sqrt{\tilde{I}(\omega - \omega_0)} \exp(i\tilde{\varphi}(\omega - \omega_0)), \quad (3)$$

where $\tilde{E}(\omega)$ is the Fourier transform of $E(t)$. $\tilde{I}(\omega - \omega_0)$ is the spectrum and $\tilde{\varphi}(\omega - \omega_0)$ is the spectral phase. The spectral phase contains time versus frequency information, and we now define the group delay versus frequency, $\tilde{t}(\omega)$ [not the inverse of $\omega(t)$], given by

$$\tilde{t}(\omega) = \frac{d\tilde{\varphi}}{d\omega}. \quad (4)$$

As in the time domain, a frequency-domain constant-phase pulse experiences no frequency variation with time (or, more precisely, time variation with frequency). Linear variation of $\tilde{\varphi}(\omega - \omega_0)$ with frequency is simply a shift in time, that is, a delay. Quadratic variation of $\tilde{\varphi}(\omega - \omega_0)$ with frequency represents a linear ramp of group delay versus frequency and corresponds to a pulse that is linearly chirped. Also, as in the time domain, higher-order terms imply nonlinear chirp.

We desire to measure $E(t)$ [or $\tilde{E}(\omega)$] completely, that is, to measure both the intensity and phase, expressed in either domain. We must be able to do so even when the pulse has significant intensity structure and highly nonlinear chirp, that is, in the general case.

Previously available technology has consisted essentially of autocorrelators and spectrometers.^{36–38} The spectrometer operates in the frequency domain and, of course, measures the spectrum. Unfortunately, it has not been possible to measure the spectral phase. In the time domain, it has not been possible to measure either $I(t)$ or $\varphi(t)$ because these pulses are so much shorter than the temporal resolution of measurement devices. The main device available for time-domain characterization of an ultrashort pulse has been the autocorrelator,^{36–38} which, since no shorter event is available, uses the pulse to measure itself. Specifically, it involves splitting the pulse into two, variably delaying one with respect to the other, and spatially overlapping the two pulses in some instantaneously responding nonlinear-optical medium, such as a second-harmonic-generation (SHG) crystal. A SHG crystal will produce light at twice the frequency of input light with an intensity that is proportional to the product of

the intensities of the two input pulses. It is clear that this yields some measure of the pulse length because no second harmonic intensity will result if the pulses do not overlap in time; thus, a relative delay of one pulse length will typically reduce the SHG intensity by about a factor of 2.

Specifically, an autocorrelator yields

$$A(\tau) = \int_{-\infty}^{\infty} I(t)I(t-\tau)dt, \quad (5)$$

where τ is the relative delay between the pulses. Unfortunately, this measurement yields a smeared out version of $I(t)$, and it often hides structure. For example, satellite pulses must be indirectly inferred from enlarged wings in $A(\tau)$. In addition, in order to obtain as little information as the pulse length, a guess must be made as to the pulse shape, yielding a multiplicative factor that relates the autocorrelation full width at half-maximum to that of the pulse $I(t)$. Unfortunately, this factor varies significantly for different common pulse shapes. This has resulted in an unfortunate temptation to choose an “optimistic” pulse shape, such as $\text{sech}^2(t)$, which yields a large multiplicative factor and hence a shorter pulse length for a given measured autocorrelation width. Also, even when the spectrum or another quantity, such as the interferometric autocorrelation,^{39–41} is also measured, there is not sufficient information to determine the pulse. Finally, systematic error can be present in the measured autocorrelation—misalignment effects that can introduce distortions—and it is difficult to know when the measured autocorrelation is free of such effects. Despite these serious drawbacks, the autocorrelation and spectrum have remained the standard measures of ultrashort pulses for over 25 years, largely for lack of better methods.

II. THE TIME-FREQUENCY DOMAIN

A large number of clever schemes have been developed over the past 25 years to better measure ultrashort laser pulses.^{42–47} Most have been novel experimental implementations and variations of autocorrelators, but many have also offered additional information about the pulse, although never full characterization. Recently, however, there has been a renaissance in this field,⁴⁸ and several new techniques have emerged that do achieve full characterization. They operate, not in the time or frequency domains, but in the “time-frequency domain.”^{30,49,50} This somewhat unintuitive domain has received much attention in acoustics research, but it has received only scant use in optics problems. Measurements in the time-frequency domain involve both temporal resolution and frequency resolution simultaneously. A well-known example of such a measurement is the musical score, which is a plot of a sound wave’s short-time spectrum versus time, with additional information on the top indicating intensity (e.g., *fortissimo* or *pianissimo*). A mathematically rigorous version of the musical score is the spectrogram:⁴⁹

$$S(\omega, \tau) = \left| \int_{-\infty}^{\infty} E(t)g(t-\tau)\exp(-i\omega t)dt \right|^2, \quad (6)$$

where $g(t-\tau)$ is a variable-delay gate function. The spectrogram is the set of spectra of all gated chunks of $E(t)$ as the delay, τ , is varied.

Knowledge of the spectrogram of $E(t)$ is sufficient to essentially completely determine $E(t)$ ^{49,51} (except for an absolute phase factor, which is of no interest in optics problems). The FROG technique involves measuring the spectrogram of the pulse.

The question that immediately arises, however, is: what gate function is available in the laboratory? It is best to use a gate that is shorter than the pulse, although not too short, or spectral information—and hence phase information—will be lost. Of course, no event shorter than the pulse is available to be used as a gate; as in an autocorrelator, it is necessary to use the pulse to gate itself. As a result, a nonlinear-optical interaction must be used to perform the gating. In fact, what is required is a spectrally resolved autocorrelator.^{17,22,52} If the signal pulse in a SHG-based autocorrelator is spectrally resolved, the result is a spectrogram:

$$I_{\text{FROG}}^{\text{SHG}}(\omega, \tau) = \left| \int_{-\infty}^{\infty} E(t)E(t-\tau)\exp(-i\omega t)dt \right|^2. \quad (7)$$

The above measurement is precisely the FROG technique using the SHG process,^{16,17,22} so we have labeled the above expression $I_{\text{FROG}}^{\text{SHG}}(\omega, \tau)$, that is, the ‘‘SHG FROG trace.’’ Other autocorrelation beam geometries are also commonly used for FROG measurements, yielding alternative types of spectrograms, and they will be discussed and compared later. In addition, we will briefly discuss the ‘‘sonogram,’’ a relative of the spectrogram, which involves gating in the frequency domain with a narrowband gate and then time resolving the gated piece of the waveform. The sonogram has also been used for ultrashort-pulse measurement.^{15,19,46,53–57}

III. PHASE RETRIEVAL

The use of the pulse to gate itself in a spectrogram complicates the problem somewhat. Spectrogram inversion algorithms require knowledge of the gate function⁵¹ and hence cannot be used. The problem must then be recast into another form. The solution is to rewrite the above expression as the ‘‘two-dimensional phase-retrieval problem.’’^{17,21,22,52}

We begin by referring to the autocorrelator signal field, $E(t)E(t-\tau)$ for an SHG autocorrelator, as $E_{\text{sig}}(t, \tau)$. Now, consider $E_{\text{sig}}(t, \tau)$ to be the Fourier transform with respect to τ (not t) of a new quantity that we will call $\hat{E}_{\text{sig}}(t, \Omega)$. It is important to note that, once found, $\hat{E}_{\text{sig}}(t, \Omega)$ easily yields the pulse field, $E(t)$. Specifically, $E(t) = \hat{E}_{\text{sig}}(t, \Omega = 0)$ (a complex multiplicative constant remains unknown, but is of little interest). Thus, to measure $E(t)$, it is sufficient to find $\hat{E}_{\text{sig}}(t, \Omega)$.

We now rewrite the expression for the FROG trace in terms of $\hat{E}_{\text{sig}}(t, \Omega)$:

$$I_{\text{FROG}}^{\text{SHG}}(\omega, \tau) = \left| \int_{-\infty}^{\infty} \hat{E}_{\text{sig}}(t, \Omega)\exp(-i\omega t - i\Omega\tau)dtd\Omega \right|^2. \quad (8)$$

This expression can be verified by simply doing the Ω integration, which then yields Eq. (7). Here, we see that the measured quantity, $I_{\text{FROG}}^{\text{SHG}}(\omega, \tau)$, is the squared magnitude of the 2D Fourier transform of $\hat{E}_{\text{sig}}(t, \Omega)$. The spectrogram measurement thus yields the magnitude, but not the phase, of

the two-dimensional Fourier transform of the desired quantity $\hat{E}_{\text{sig}}(t, \Omega)$. The problem is then to find the phase of the Fourier transform of $\hat{E}_{\text{sig}}(t, \Omega)$. This is the 2D phase-retrieval problem.⁵⁸

Quite unintuitively, this is a solved problem when certain additional information regarding $\hat{E}_{\text{sig}}(t, \Omega)$ is available, such as that it has finite support (that is, is zero outside a finite range of values of t and Ω).^{58–61} This is in contrast to the 1D problem, in which it is impossible to find a function of one variable whose Fourier-transform magnitude is known, despite additional information, such as finite support. Indeed, in the 1D case, infinitely many additional solutions exist.^{58,62,63} The two-dimensional phase-retrieval problem occurs frequently in imaging problems,^{61,64} where finite support is common. In ultrashort-pulse measurement, the required additional information consists, not of finite support, but of the knowledge of the mathematical form of $\hat{E}_{\text{sig}}(t, \Omega)$. For example, in SHG FROG,¹⁶ we know that $E_{\text{sig}}(t, \tau) = E(t)E(t-\tau)$. In another version of FROG, called polarization-gate (PG) FROG,¹⁷ $E_{\text{sig}}(t, \tau) = E(t)|E(t-\tau)|^2$. This additional information turns out to be sufficient, and thus, the problem is solved.¹⁷ Indeed, it is solved in a particularly robust manner, with many other advantageous features, such as feedback regarding the validity of the data.^{23,32,34} In Sec. VII, we will discuss the algorithm that finds the solution to the two-dimensional phase-retrieval problem for ultrashort-laser-pulse measurement in detail.

IV. A BRIEF HISTORY OF ULTRASHORT-LASER-PULSE MEASUREMENT

The first use of time-frequency methods for ultrashort-laser-pulse characterization was by Treacy in 1971,⁶⁵ who made sonograms of ultrashort pulses but did not retrieve the intensity and phase from them. Unfortunately, this work does not appear to have been appreciated at this time, and the final step of pulse retrieval from these sonograms was not taken. These ideas were rediscovered only recently.^{46,53,54} Chilla and Martinez were the first to retrieve (approximately) the full intensity and phase of an ultrashort pulse from a sonogram.^{15,55,56} Others have since developed variations on their method.^{19,57} Ishida and co-workers were, to our knowledge, the first to make spectrograms of ultrashort laser pulses, but they did not retrieve pulses from them.^{66–68} Trebino and Kane^{17,21,22,52} introduced phase-retrieval techniques and were the first to develop a rigorous method (FROG) for pulse characterization. In this work, we will concentrate on FROG. FROG is the most studied and established ultrashort-pulse measurement technique, and it has all of the advantages mentioned in Sec. I, while other techniques do not. It also makes explicit use of phase retrieval, which is responsible for its accuracy and versatility, while other methods do not and, as a result, achieve at best approximate results for simple pulses only.

V. FROG: GENERAL FEATURES

FROG is any autocorrelation-type measurement in which the autocorrelator signal beam is spectrally resolved (see Figs. 1 and 2).^{17,21,22,52} Because several different beam

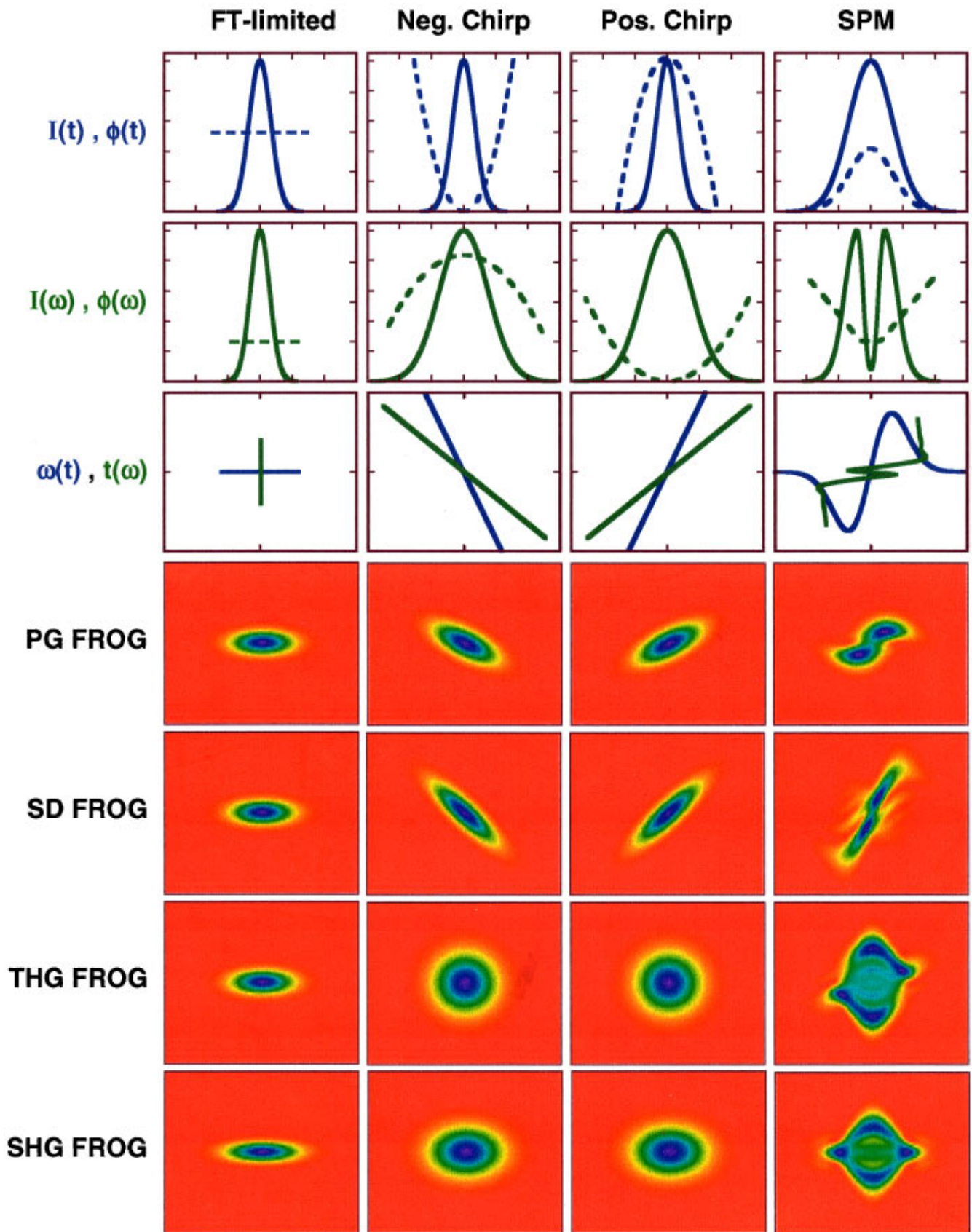


FIG. 2. FROG traces for the various FROG geometries for typical ultrashort light pulses. The top row shows the intensity vs time, $I(t)$ (solid line), and phase vs time, $\phi(t)$ (dashed line), for various pulses. The next row shows the spectrum, $\tilde{I}(\omega - \omega_0)$ (solid line), and the spectral phase, $\tilde{\phi}(\omega - \omega_0)$ (dashed line), for each pulse. In the first two rows of plots in this figure, the ticks on the phase axis correspond to increments of π radians. The third row shows the instantaneous frequency vs time, $\omega(t)$ (in blue). Also shown in the third row is the group delay vs frequency, $\tilde{t}(\omega)$ (in green). Note that the $\tilde{t}(\omega)$ plots must be turned sideways because the horizontal axis in this row of figures is time, and the vertical axis is frequency. Arrows in this figure indicate infinities. The remaining four rows show false-color (purple means high intensity and red means low intensity) FROG traces for the various pulses for the different FROG beam geometries: polarization gate (PG), self-diffraction (SD), second-harmonic generation (SHG), and third-harmonic generation (THG). Note that no row exists for transient grating (TG) FROG because it yields traces that are identical to PG FROG or SD FROG, depending on which pulse is delayed. Note that the PG and SD FROG traces mirror the instantaneous frequency vs time or the group delay vs frequency, whichever is more intuitive. The THG FROG traces are more symmetrical, and hence less intuitive, and the SHG FROG traces are perfectly symmetrical and hence have an ambiguity in the direction of time.

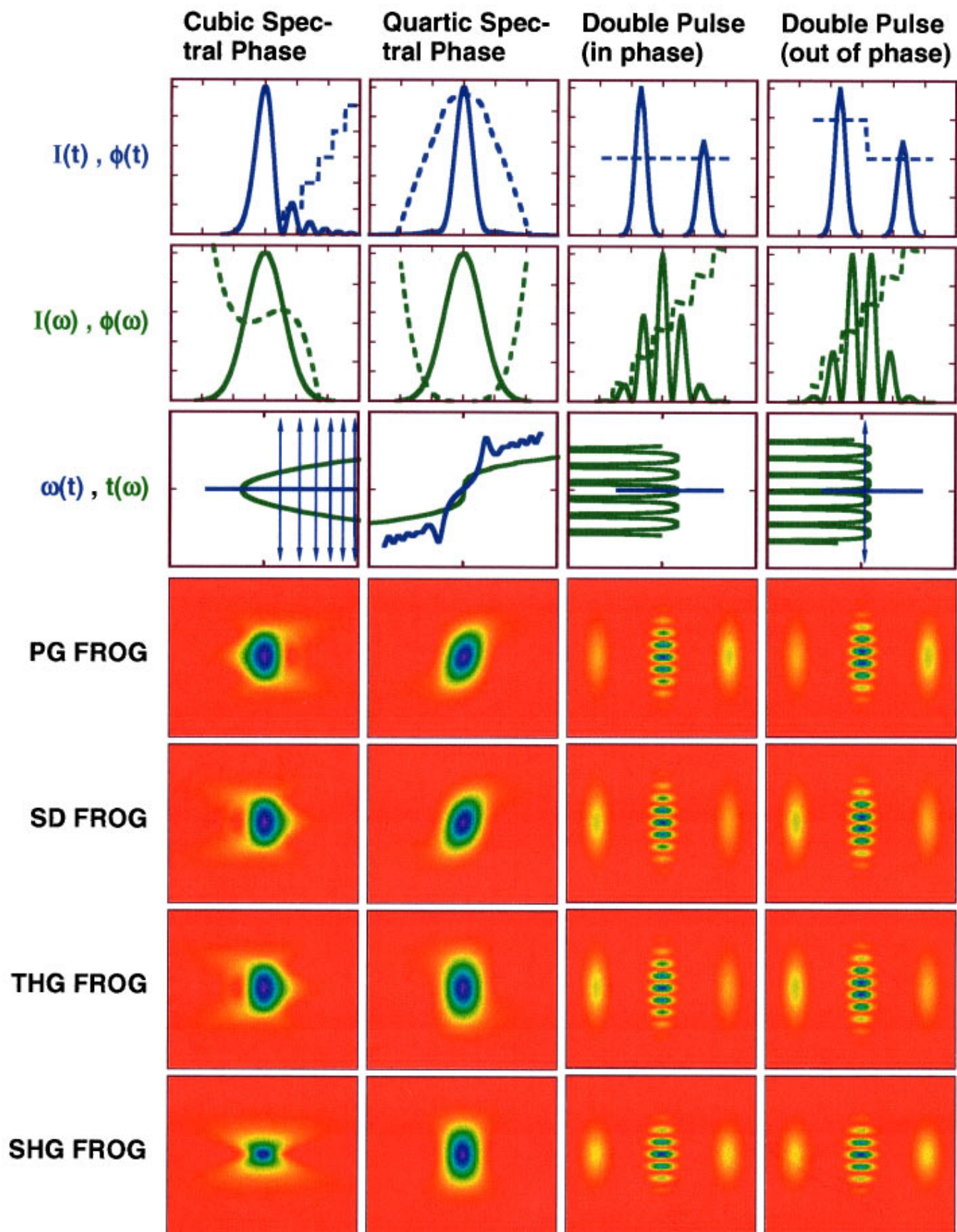


FIG. 2 (Continued.)

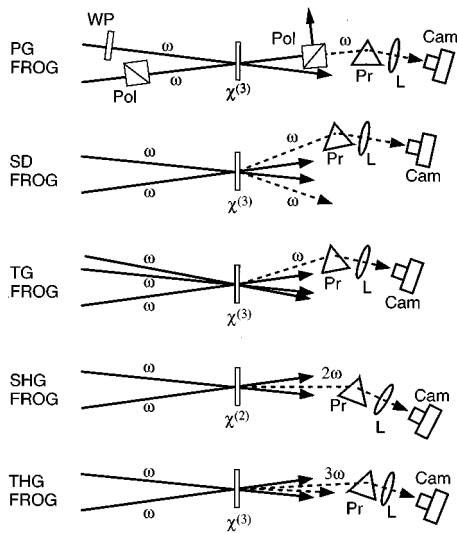


FIG. 1. Schematics of five different beam geometries for performing FROG measurements of ultrashort laser pulses: polarization gate (PG), self-diffraction (SD), second-harmonic generation (SHG), and third-harmonic generation (THG), and transient grating (TG) FROG. Solid lines indicate input pulses, and dashed lines indicate signal pulses. The nonlinearity of the nonlinear medium is shown; Pol=polarizer; WP=wave plate; Pr=prism; L=lens; and Cam=Camera. The prism-lens combination in each arrangement is meant to represent a generic spectrometer, which could involve a grating or other dispersive element instead of the prism. Not shown are delay lines and various additional lenses, also common to all arrangements. The frequencies shown (ω , 2ω , 3ω) are the carrier frequencies of the pulses involved and indicate whether the signal pulse has the same carrier frequency as the input pulse or is shifted, as in SHG and THG.

geometries can be used for performing autocorrelation measurements, there are also several beam geometries for performing FROG measurements, and they are illustrated in Fig. 1, and some of their properties are summarized in Table I. Each yields its own traces, although some geometries yield similar traces, and learning to read them is easy if one remembers that they are essentially musical scores of the pulse. Measured traces for various pulses are shown in Fig. 2. The pulse intensity and phase may be estimated simply by looking at the experimental trace, or the iterative algorithm may be used to retrieve the precise intensity and phase versus time or frequency (usually in a few seconds to a minute). Before we discuss these geometries in detail, however, we describe several general features of FROG.

Unlike other ultrashort-pulse-measurement methods, FROG is very accurate. No approximations are made. All that must be assumed in FROG is a nearly instantaneously responding medium, and even that assumption has been shown to be unnecessary, as the medium response can be included in the algorithm.⁶⁹ Similarly, any known systematic error in the measurement may also be modeled in the algorithm,^{32,34} although this is not generally necessary, except for extremely short pulses (< 10 fs).

Also, unlike other ultrashort pulse measurement methods, FROG completely determines the pulse with essentially infinite temporal resolution.^{21,32} It does this by using the time domain to obtain long-time resolution and the frequency domain for short-time resolution. As a result, if the full pulse spectrogram is entirely contained within the measured trace, then there can be no additional long-time pulse structure

TABLE I. Brief summary of the characteristics of the various FROG beam geometries. Single-shot and multishot sensitivity values are very rough and assume 800 nm, 100 fs pulses from a regeneratively amplified or unamplified Ti:sapphire oscillator, respectively, using a weak focus to about 100 μm in the nonlinear medium. Tighter focus (~ 10 μm) is assumed in THG FROG because the nonlinearity assumed for this table is a surface effect, and the resulting decrease in Rayleigh range results in no loss of signal.

Geometry	PG	SD	TG	THG	SHG
Nonlinearity	$\chi^{(3)}$	$\chi^{(3)}$	$\chi^{(3)}$	$\chi^{(3)}$	$\chi^{(2)}$
Sensitivity (single shot)	$\sim 1 \mu\text{J}$	$\sim 10 \mu\text{J}$	$\sim 0.1 \mu\text{J}$	$\sim 0.03 \mu\text{J}$	$\sim 0.01 \mu\text{J}$
Sensitivity (multishot)	$\sim 100 \text{ nJ}$	$\sim 1000 \text{ nJ}$	$\sim 10 \text{ nJ}$	$\sim 3 \text{ nJ}$	$\sim 0.001 \text{ nJ}$
Advantages	Intuitive traces; Automatic phase matching	Intuitive traces	Bkgrnd-free; Sensitive; Intuitive traces	Sensitive; Very large bandwidth	Very sensitive
Disadvantages	Requires polarizers	Requires thin medium; not phase matched	Three beams	Unintuitive traces; Very short- λ signal	Unintuitive traces; Short- λ signal
Ambiguities	None known	None known	None known	Relative phase of multiple pulses: $\varphi, \varphi \pm 2\pi/3$	Direction of time; Rel. phase of multiple pulses: $\varphi, \varphi + \pi$

(since the spectrogram is essentially zero for off-scale delays), and there can be no additional short-time pulse structure (since the spectrogram is essentially zero for off-scale frequency offsets). Interestingly, this extremely high temporal resolution can be obtained by using delay increments that are as large as the time scale of the structure. Again, this is because the short-time information is obtained from large frequency-offset measurements. Thus, as long as the measured FROG trace contains all of the nonzero values of the pulse FROG trace, the result is rigorous. (Of course, the trace typically only falls asymptotically to zero as it extends to delays and frequency offsets of $\pm\infty$ in all directions, but these low values outside the measured trace do not significantly affect the retrieved pulse.)

Another useful and important feature that is unique to FROG is the presence of feedback regarding the validity of the measurement data. FROG actually contains two different types of feedback. The first is probabilistic, rather than deterministic, but it is still helpful. It results from the fact that the FROG trace is a time-frequency plot, that is, an $N \times N$ array of points, which are then used to determine N intensity points and N phase points, that is, $2N$ points. There is thus significant overdetermination of the pulse intensity and phase—there are many more degrees of freedom in the trace than in the pulse. As a result, the likelihood of a trace composed of randomly generated points corresponding to an actual pulse is very small. Similarly, a measured trace that has been contaminated by systematic error is unlikely to correspond to an actual pulse. Thus, convergence of the FROG algorithm to a pulse whose trace agrees well with the measured trace virtually assures that the measured trace is free of systematic error. Conversely, nonconvergence of the FROG algorithm (which rarely occurs for valid traces) indicates the presence of systematic error. To appreciate the utility of this feature, recall that intensity autocorrelations have only three constraints: a maximum at zero delay, zero for large delays, and even symmetry with respect to delay. These constraints do not limit the autocorrelation trace significantly, and one commonly finds that the autocorrelation trace can vary quite a bit in width during alignment while still satisfying these constraints. Other intensity-and-phase methods measure a time-frequency-domain plot, but they use only the mean delay versus frequency or similar quantity and, as a result, also lack this feedback. It should be emphasized that this argument is merely probabilistic, and that, on one occasion, we encountered a systematic-error-contaminated SHG FROG trace that yielded convergence. However, the SHG FROG trace has additional symmetry that is lacking in other FROG methods, so such an occurrence is more likely there. The other FROG methods have so far reliably revealed systematic error in this manner.

Another feedback mechanism in FROG is deterministic and has proven extremely effective in revealing systematic error in SHG FROG measurements of ~ 10 fs pulses, where crystal phase-matching bandwidths are insufficient for the massive bandwidths of the pulses to be measured. It involves computing the “marginals” of the FROG trace, that is, integrals of the trace with respect to delay or frequency. The marginals can be compared to the independently measured

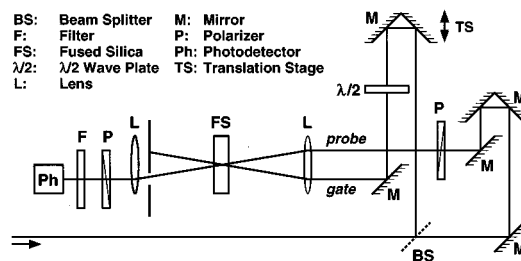


FIG. 3. Experimental apparatus for multishot PG FROG measurements.

spectrum or autocorrelation, and expressions have been derived relating these quantities. Comparison with the spectrum is especially useful. The marginals can even be used to correct an erroneous trace. The interested reader is referred to the relevant references for more detail on this subject.^{23,32,34}

VI. THE FROG APPARATUS: BEAM GEOMETRIES

In this section, we describe and compare several FROG beam geometries and their traces, so that the choice of which geometry to use may be more easily made. We also give sufficient detail to set up several of them.

A. Polarization-gate FROG

Polarization-gate (PG) FROG^{17,21,23,24,35,70} uses the polarization-gate beam geometry, popular for optical gating and shown in Fig. 1 and in greater detail in Fig. 3. In this geometry, the pulse is split into two, with one pulse (the “probe”) then sent through crossed polarizers and the other (the “gate”) through a half-wave plate or other device in order to achieve a ± 45 deg linear polarization with respect to that of the probe pulse. The two pulses are then spatially overlapped in a piece of fused silica (or other medium with a very fast third-order susceptibility). In the fused silica, the gate pulse induces a birefringence through the electronic Kerr effect, a third-order optical nonlinearity, also known as the nonlinear refractive index. As a result, the fused silica acts as a wave plate while the gate pulse is present, rotating the probe pulse’s polarization slightly, which allows some light to be transmitted through the analyzer. Because birefringence occurs only when the gate pulse is present, this geometry yields an autocorrelation measurement of the pulse if one simply measures the energy of the light transmitted through the analyzer versus the relative delay between the two pulses. And by spectrally resolving the light transmitted by the analyzer versus delay, a PG FROG trace is measured.

The PG FROG trace is given by

$$I_{\text{FROG}}^{\text{PG}}(\omega, \tau) = \left| \int_{-\infty}^{\infty} E(t) |E(t - \tau)|^2 \exp(-i\omega t) dt \right|^2. \quad (9)$$

Note that the gate function in PG FROG is $|E(t - \tau)|^2$, which is a real quantity and so adds no phase information to the gated slice of $E(t)$ whose spectrum is measured. As a result, PG FROG traces are quite intuitive, accurately reflecting the pulse frequency versus time. Sample PG FROG traces are shown in Fig. 2.

PG FROG is the most intuitive FROG variation, and it has many other desirable qualities. First, and most importantly, there are no known ambiguities in PG FROG. Thus, PG FROG yields complete and unambiguous pulse characterization in all known cases.

This lack of ambiguities is quite useful, but it is also interesting because it is well known that the spectrogram—which is different from FROG in that it uses an independent gate function (i.e., not a gate consisting of the pulse itself, as in FROG)—has an ambiguity in the relative phase of well separated pulses. For such an independent-gate spectrogram, the relative phase of well separated pulses is completely undetermined. This is because, when the two pulses are separated by more than the gate width, the spectrogram splits into the sum of the two individual-pulse spectrograms, and the squared magnitude prevents the determination of the relative phase. There are thus infinitely many different relative-phase values possible in the independent-gate spectrogram of well-separated pulses. This ambiguity does not occur in PG FROG [or any other FROG variation, although SHG FROG has a single ambiguity, φ and $\varphi + \pi$, and third harmonic generation (SHG) FROG has a double ambiguity, φ and $\varphi \pm 2\pi/3$, in the relative phase of such pulses for other reasons] because, in FROG, the gate is the pulse itself, so the pulses cannot be separated by more than the gate width.

Another advantage of PG FROG is that the nonlinear-optical process is automatically phase matched, so alignment is easy.

Disadvantages of PG FROG are that it requires high-quality polarizers (an extinction coefficient of better than 10^{-5} is recommended), which can be expensive. In addition, high-quality polarizers tend to be fairly thick, so pulses can change due to material dispersion while propagating through them. This is not as problematic as it first appears because the full pulse intensity and phase are measured at the fused silica, so it is possible to theoretically propagate the pulse to any point before or after the point where it was measured. Nevertheless, this is somewhat undesirable. A further disadvantage of the requirement of high-quality polarizers is that they are unavailable in spectral regions such as the deep UV ($< \sim 250$ nm). They also limit sensitivity because there is always some leakage.

These disadvantages are not severe, however, especially for amplified ultrashort pulses in the visible and the near-IR. And to date, the PG FROG technique has been used by many groups to perform multishot and single-shot measurements of ultrashort pulses, and a commercial PG FROG product is currently available.

Typical values of the various optical elements in a multishot PG FROG device for measuring amplified 100 fs, 800 nm, > 100 nJ pulses from a regeneratively amplified Ti:sapphire laser are as follows.⁷⁰ A 50% beam splitter splits the pulse to be measured into two, one of which passes through crossed calcite polarizers (extinction coefficient $< 10^{-5}$), the other of which is polarization rotated by a wave plate (or out-of-plane propagation) to a ± 45 -degree (or circular) polarization. The pulses, lightly focused using a ~ 50 cm lens, overlap in an approximately 1-mm-thick piece of fused silica. The light passing through the second polarizer is the

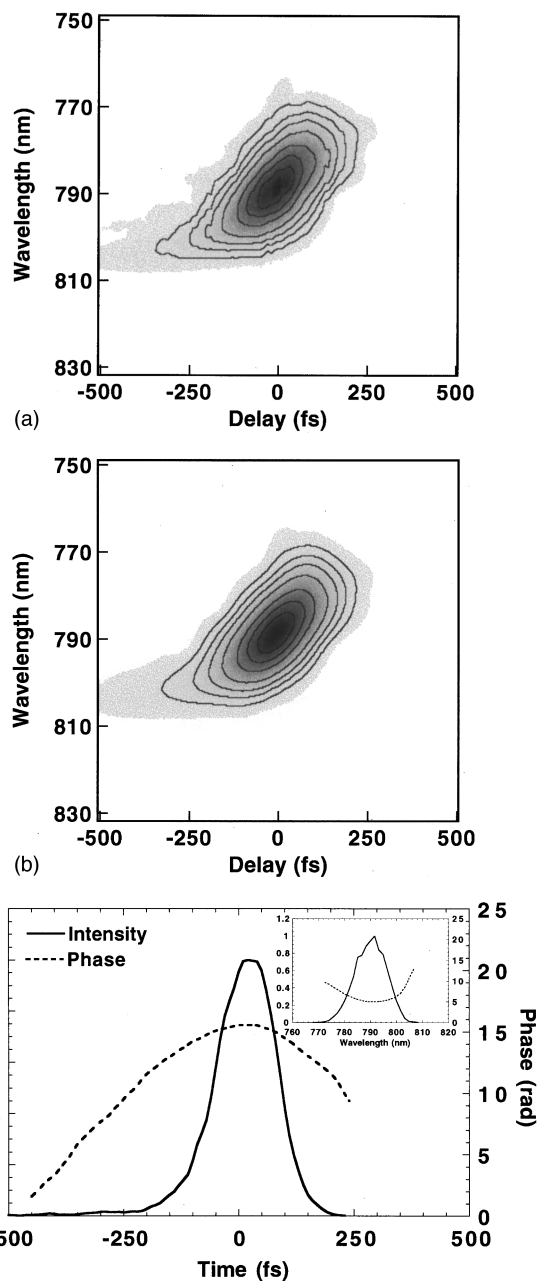
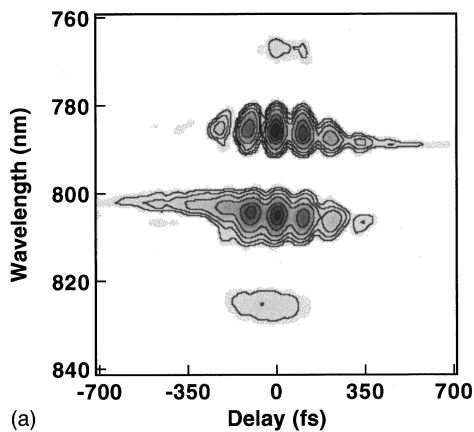
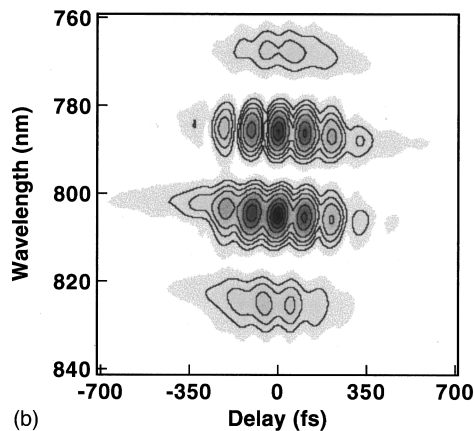


FIG. 4. (a) Experimental multishot FROG trace for an ultrashort laser pulse with positive linear chirp. (b) FROG trace for the pulse retrieved by the algorithm. (c) Retrieved intensity and phase. Note the similar pulse intensity and phase to that shown in Fig. 2 for a linearly chirped pulse. In Figs. 4 and 5, contour lines represent the values: 2%, 5%, 10%, 20%, 40%, 60%, and 80%.

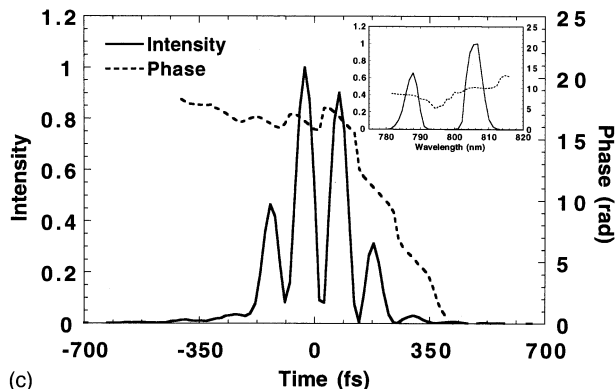
signal pulse, and it is sent into a 1/4 m spectrometer incorporating a ~ 1200 line per mm diffraction grating. A homemade spectrometer, using a grating and a pair of lenses also works well (the focus in the fused silica can function as the entrance slit). A video or CCD camera at the output plane of the spectrometer then measures the spectrum averaged over as many as 1000 pulses. The delay of one of the two pulses is then varied using a delay line, and the spectrum is measured for about 100 different delays, a few femtoseconds apart. The above spectrometer yields more than sufficient spectral resolution for measurements of ~ 100 fs pulses, and it may be necessary to combine adjacent spectral values to



(a)



(b)



(c)

FIG. 5. (a) Experimental multishot FROG trace for a shaped (multiple pulse) ultrashort laser pulse. (b) FROG trace for the pulse retrieved by the algorithm. (c) Retrieved intensity and phase. Note that FROG is able to retrieve a pulse that is quite complex. (Discrepancies between the measured and retrieved traces are probably due to spatial inhomogeneities in the beam.)

reduce the number of points per spectrum. Indeed, for the measurement of significantly shorter pulses, a prism spectrometer may be used.^{29,34} Figures 4 and 5 show typical experimental PG FROG traces and the retrieved pulse intensities and phases for two different ultrashort pulses. These measurements were made by Kohler, Wilson, and co-workers,⁷⁰ who routinely make complex shaped pulses for the control of chemical reactions.

PG FROG is easily implemented in a single-shot beam geometry, which can yield measurement of a single ultrashort laser pulse. This is achieved by focusing the two beams with a cylindrical lens and crossing them at a fairly

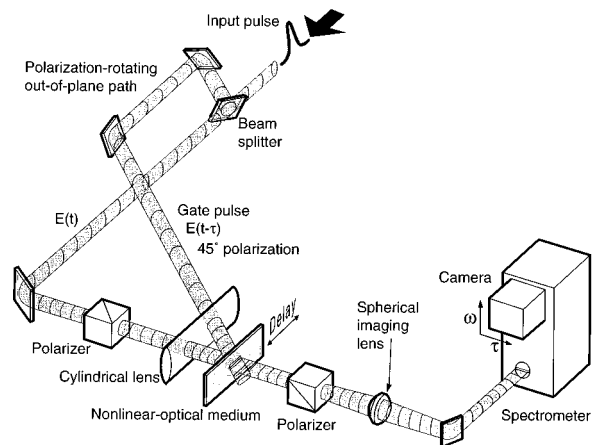


FIG. 6. Experimental apparatus for single-shot PG FROG [from Kane and Trebino (Ref. 21)]. In order to perform a single-shot measurement, the beams are crossed at a large angle (10–20 deg) and focused with a cylindrical lens, yielding a line focus in the nonlinear medium, where the relative delay between the two pulses varies with spatial coordinate along the line focus. This focus is then imaged onto the entrance slit of the spectrometer, whose output yields the entire FROG trace on a single shot. In this apparatus, the out-of-plane propagation of one of the beams is to rotate the polarization of the beam by about 45 deg.

large angle, say, about 10 deg. In this manner, the relative delay between the pulses varies with position at the fused silica nonlinear medium. A spherical lens then images the line-shaped beam-overlap region at the fused silica onto the entrance slit of the spectrometer, so that delay is then mapped onto position along this slit. The optics of the spectrometer then image this delay variation onto the exit plane of the spectrometer (shown on its side in Fig. 6), delay proceeds horizontally and frequency proceeds vertically, and the entire trace is obtained on each laser shot.

In such a single-shot geometry, any focusing of the beams into the fused silica nonlinear medium should be performed with a cylindrical lens because the range of delays achievable in this manner is proportional to the spot size in the plane of the beams, and several mm spot sizes are typically required to achieve a few hundred fs of delay. It is essential, in using this type of beam geometry, to maintain excellent spatial beam quality, and spatial filtering of the beams before the FROG device is recommended. Single-shot operation is easily achieved with all FROG beam geometries in a similar manner. It should be mentioned that such measurements require the use of an imaging spectrometer, that is, a spectrometer that images the entrance slit onto a focused and untilted slit at the exit plane. Because off-axis reflections are usually used in commercial spectrometers, they typically are not of this type, unless specifically designed, usually with aspherics, to be so. Interestingly, the typical “home-brew” spectrometer, constructed using a pair of lenses and a grating or prism (see Fig. 1), is, in fact, an imaging spectrometer, provided that on-axis propagation occurs at both lenses. Single-shot PG FROG experiments have been performed on visible and 308 nm UV pulses by Kane and Trebino.^{21,24}

In all versions of FROG, beam angles should be as small as is acceptable in view of scattered light and, if single shot,

the required range of delays. Otherwise, a geometrical smearing effect can artificially broaden the pulse in time. This effect was described for single-shot PG FROG by Tien *et al.*⁷¹ and DeLong *et al.*,³² and for multishot PG FROG by Taft *et al.*³⁴ but also can occur in all versions of FROG as well as in other pulse-measurement techniques.

Finally, recall that PG FROG utilizes a third-order nonlinearity, so the signal intensity scales as the third power of the input intensity. Consequently, pulses that are longer or weaker by a factor of 2 yield one eighth the output power. And an increase in the spot size by a factor of 2 yields one sixty-fourth the signal intensity. The same is, of course, true for other third-order FROG and autocorrelation methods.

B. Self-diffraction FROG

Self-diffraction (SD)^{22,31} is another beam geometry that uses the electronic Kerr effect as the nonlinear-optical process for making optical gating in FROG measurements (see Fig. 1). SD FROG also involves crossing two beams in a piece of fused silica (or other third-order nonlinear medium), but in SD FROG, the beams can have the same polarizations. The beams generate a sinusoidal intensity pattern and hence induce a material grating, which diffracts each beam into the directions shown in Fig. 1. Spectrally resolving one of these beams as a function of delay yields an SD FROG trace, examples of which are shown in Fig. 2. The expression for the SD FROG trace is

$$I_{\text{FROG}}^{\text{SD}}(\omega, \tau) = \left| \int_{-\infty}^{\infty} E(t)^2 E(t-\tau)^* \exp(-i\omega t) dt \right|^2. \quad (10)$$

SD FROG traces differ slightly from PG FROG traces.²³ For a linearly chirped pulse, the slope of the SD FROG trace is twice that of the PG FROG trace.²³ As a result, SD FROG is more sensitive to this and other even-order temporal-phase distortions. It is, however, less sensitive to odd-order temporal-phase distortions. SD FROG also uniquely determines the pulse intensity and phase.

An advantage of SD FROG over PG FROG is that it does not require polarizers, so it can be used for deep UV pulses or pulses that are extremely short, for which high-quality polarizers are unavailable or undesirable. On the other hand, SD is not a phase-matched process. As a result, the nonlinear medium must be kept thin ($< \sim 200 \mu\text{m}$) and the angle between the beams small ($< \sim 2 \text{ deg}$) in order to minimize the phase mismatch. In addition, the phase mismatch is wavelength dependent. Consequently, if the pulse bandwidth is large, the SD process can introduce wavelength-dependent inefficiencies into the trace, resulting in distortions. These pitfalls are easily avoided for ≥ 100 fs pulses, and Clement and co-workers have shown that SD FROG is a good method for measuring amplified ultrashort pulses in the violet on a single shot.³¹

C. Transient-grating FROG

Ideally, one would like a beam geometry that is both phase matched and free of polarizers. The transient-grating (TG) beam geometry (see Figs. 1 and 7) is such a geometry, and we consider it to be the best all-round beam geometry

for FROG measurements of amplified ultrashort pulses.⁷² Indeed, the TG geometry is very popular in nonlinear-spectroscopy measurements,⁷³⁻⁷⁵ also, and its advantages for such measurements are also advantages for FROG measurements.

TG FROG is a three-beam geometry, requiring that the input pulse be split into three pulses. Two of the pulses are overlapped in time and space at the optical-Kerr medium, producing a refractive-index grating, just as in SD FROG. In TG, however, the third pulse is variably delayed and overlapped in the fused silica and is diffracted by the induced grating to produce the signal pulse. The four beam angles (three input and one output) in TG geometries usually take the form of what is known as the BOXCARS arrangement,⁷⁶ in which all input pulses and the signal pulse are nearly collinear, but appear as spots in the corners of a rectangle on a card placed in the beams. While nonlinear spectroscopists often use an arrangement in which two beams nearly counterpropagate with the other two,^{77,78} all four beams should nearly copropagate in FROG measurements in order to avoid temporal smearing effects due to large beam angles.

Depending on which pulse is variably delayed (with the other two coincident in time), the TG FROG trace is mathematically equivalent to PG FROG or SD FROG. To see this, note that if pulse No. 2 in Fig. 7 is variably delayed, the signal pulse is given by

$$E_{\text{sig}}^{\text{TG1}}(t, \tau) = E_1(t) E_2^*(t-\tau) E_3(t). \quad (11)$$

Since all pulses are identical, this becomes

$$E_{\text{sig}}^{\text{TG1}}(t, \tau) = E(t)^2 E^*(t-\tau), \quad (12)$$

which is just the expression for the SD FROG signal field. An analogous argument shows that if either of the other two pulses is variably delayed, the signal field is identical to the PG FROG signal field (with a reversed sign of the delay). Thus, TG FROG yields familiar traces.

TG FROG has several advantages over its two-beam cousins. Unlike PG FROG, it avoids polarizers, so it does not distort extremely short pulses, and hence can be used in the deep UV. More importantly, it is background-free. It can use all parallel polarizations, which yields greater signal strength because the $\chi_{1111}^{(3)}$ element of the susceptibility tensor is a factor of three larger than the off-diagonal elements used in PG FROG. This fact, coupled with the lack of polarizer-leakage background, makes TG FROG significantly more sensitive than PG FROG. Unlike SD FROG, TG FROG is phase matched, so long interaction lengths in the nonlinear medium may be used, enhancing signal strength due to the length-squared dependence of the signal. In addition, larger beam angles may be used than in SD FROG, reducing any scattered-light background. As a result, TG FROG is also significantly more sensitive than SD FROG. At the same time, TG FROG retains the intuitive traces and ambiguity-free operation common to these two-beam FROG methods. The only disadvantage of TG FROG is the need for three beams and to maintain good temporal overlap of the two constant-delay beams. But we have found these requirements not to be particularly inconvenient, and the advantages of this geometry far outweigh the disadvantages. For example,

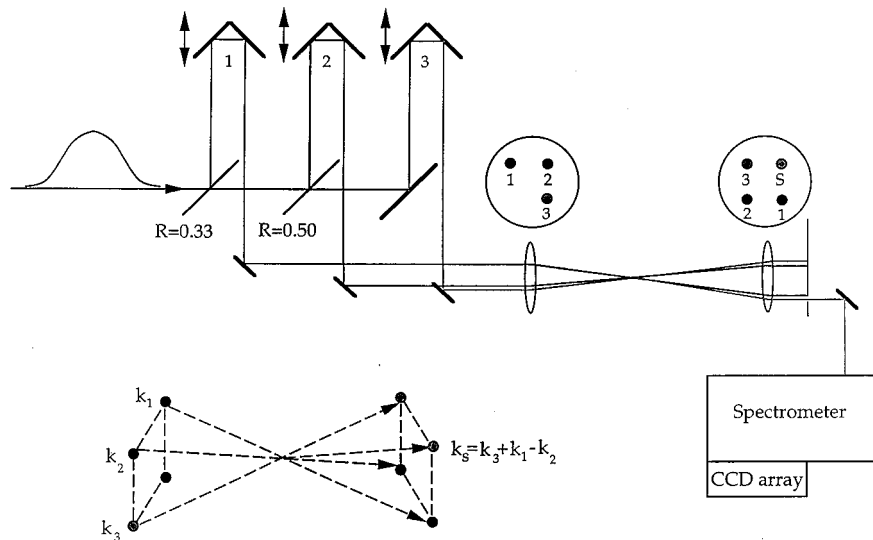


FIG. 7. Experimental apparatus for TG FROG (from Sweetser *et al.* Ref. 72). The input pulses are numbered 1, 2, and 3, and “s” indicates the signal pulse. A “BOXCARS” beam geometry is best, in which each pulse propagates at the corner of a rectangle. All pulses should propagate in nearly the same direction to avoid temporal smearing. Two pulses should be coincident in time, while the other has variable delay. The inset shows the phase-matching condition.

the large bandwidth of this entirely phase-matched geometry and the avoidance of potentially pulse-distorting polarizers make TG FROG ideal for measuring extremely short pulses (~ 20 fs) of a few tens of nJ or more. Indeed, Rundquist and co-workers have made such measurements with excellent results.

D. Second-harmonic-generation FROG

We have already mentioned the SHG FROG method. Figures 1 and 8 show schematics of this method. The main advantage of SHG FROG is sensitivity: it involves only a second-order nonlinearity, while the previously mentioned FROG variations use third-order optical nonlinearities, which are much weaker. As a result, for a given amount of input pulse energy, SHG FROG will yield more signal pulse energy. SHG FROG is commonly used to measure unamplified pulses directly from a Ti:sapphire oscillator, and it can measure pulses as weak as about 1 pJ; it is only slightly less sensitive than an autocorrelator.

The main disadvantages of SHG FROG are that, unlike the previously mentioned third-order versions of FROG, it has an unintuitive trace that is symmetrical with respect to delay, and, as a result, it has an ambiguity in the direction of

time. The pulse, $E(t)$, and its time-reversed replica, $E(-t)$, both yield the same SHG FROG trace. Thus, when an SHG FROG trace is measured and the phase-retrieval algorithm run on it, it is possible that the actual pulse is the time-reversed version of the retrieved pulse. This ambiguity can easily be removed in one of several ways. One is to make a second SHG FROG measurement of the pulse after distorting it in some known manner. The most common method is to place a piece of glass in the beam (before the beam splitter), introducing some positive dispersion and hence chirp into the pulse. Only one of the two possible pulses is consistent with both measurements. (Placing a piece of glass after the beam splitter—in only one beam—and measuring only a single SHG FROG trace is not sufficient to remove this ambiguity, unless traces using two different elements are made.) Another is to know in advance something about the pulse, such as that it is positively chirped. And finally, Taft³⁴ has found that placing a thin piece of glass in the pulse before the beam splitter so that surface reflections introduce a small trailing satellite pulse also removes the ambiguity. This method has the advantage of requiring only one SHG FROG trace measurement to determine the pulse (the time-reversed pulse in this case has a leading satellite pulse).

Despite the existence of a “proof”⁷⁹ that the only ambiguity in SHG FROG is the direction of time, we have also recently discovered another class of ambiguities in SHG FROG. These ambiguities rarely appear in practical measurements but are worth mentioning. If the pulse consists of two (or more) well separated pulses, then the relative phase of the pulses has an ambiguity. Specifically, the relative phases, φ and $\varphi + \pi$, yield the same SHG FROG trace and hence cannot be distinguished. Note that this ambiguity also occurs when one measures the simple spectrum of the pulse pair, so adding the spectrum to the SHG FROG trace does not remove it (the information contained in the spectrum is con-

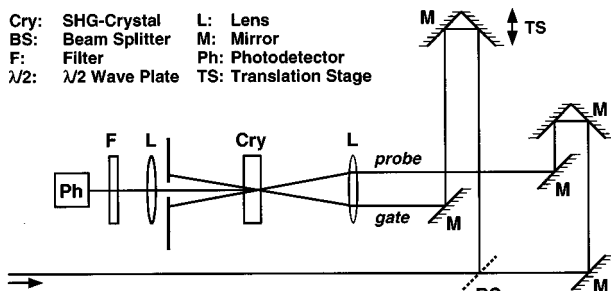


FIG. 8. Experimental apparatus for multishot SHG FROG.

tained in the SHG FROG trace anyway). This ambiguity is less severe than and should be distinguished from the ambiguity mentioned earlier in spectrograms using an independent gate (i.e., not FROG), which is a complete indeterminacy of the relative phase between well separated pulses.

The most important experimental consideration in SHG FROG is that the SHG crystal have sufficient bandwidth (i.e., be thin enough, since the bandwidth is inversely proportional to the crystal thickness) to frequency double the entire bandwidth of the pulse to be measured. If the crystal is too thick, then the SHG FROG trace will be too narrow along the spectral axis, leading to nonconvergence of the algorithm. It is important to realize that autocorrelators carry the same crystal-bandwidth requirement, but this requirement is often violated in practice because, unlike FROG, no independent check of the autocorrelation trace exists. Also, a very convenient feature of FROG is that it is possible to correct for this effect.³⁴ SHG FROG has been discussed in detail in other work.^{16,17,21,23,29,34,79}

Figure 9 shows a typical SHG FROG apparatus, consisting of a 50% beam splitter, a delay line using two mirror pairs (or corner cubes) on translation stages to give variable delays, a 10- to 50-cm-focal-length lens or mirror to focus the pulses into the SHG crystal [usually potassium dihydrogen phosphate (KDP) or (BBO)], and a 1/8 to 1/4 m spectrometer/camera. A filter blocks the fundamental-frequency light, although this is also done by the spectrometer. As in autocorrelation and other pulse-measurement methods, the crystal thickness for measuring 100 fs, 800 nm pulses should be no more than $\sim 300 \mu\text{m}$ for KDP and $\sim 100 \mu\text{m}$ for BBO. Figure 9 shows an experimental SHG FROG trace for a pulse with very small satellite pulses, the retrieved FROG trace, and the retrieved intensity and phase. Note the good agreement between experimental and retrieved traces, even at the $\sim 10^{-4}$ level. The retrieved pulse yields a FROG error (the rms error between experimental and retrieved traces; see Sec. VII for further discussion of the FROG error) of 0.0016, indicative of a very accurate measurement. We also refer the reader to the excellent recent work of Dudley and co-workers, who have used SHG FROG to measure exceedingly complex pulses resulting from propagation through 700 m of fiber.⁸⁰

E. Third-harmonic-generation FROG

It is also possible to use third-harmonic generation (THG) as the nonlinear-optical process in a FROG apparatus. This has been done by Tsang *et al.*, using surface THG (STHG),⁸¹ a surprisingly strong effect, which has allowed the measurement of unamplified pulses from a Ti:sapphire oscillator. Figures 1 and 10 show the arrangement for THG FROG.

The expression for the THG FROG trace is

$$I_{\text{FROG}}^{\text{THG}}(\omega, \tau) = \left| \int_{-\infty}^{\infty} E(t)^2 E(t - \tau) \exp(-i\omega t) dt \right|^2, \quad (13)$$

which is similar to that of SHG FROG, except that one of the factors is squared. There are two possible signal beams that can be spectrally resolved in THG FROG measurements, and the choice of these beams determines which factor of the

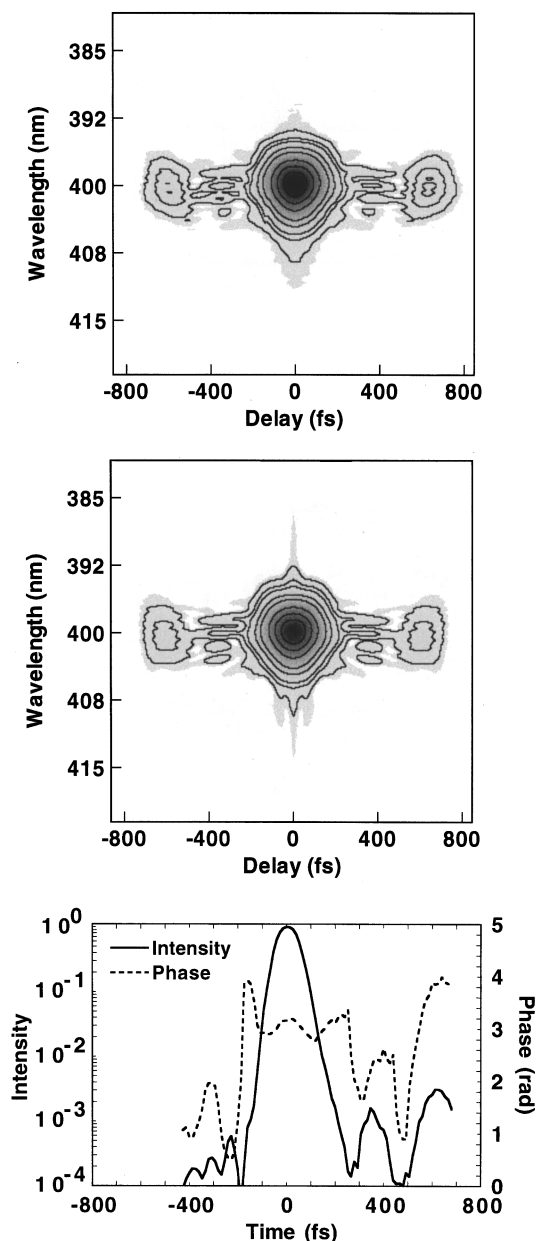


FIG. 9. (a) Experimental multishot SHG FROG trace for a pulse from an unamplified Ti:sapphire oscillator. In order to illustrate the large dynamic range of SHG FROG, we have plotted the square root of the FROG intensity, which emphasizes the small details and weak satellite pulses. In addition, the contour lines indicate the values 2%, 4%, 6%, 12%, 20%, 40%, 60%, and 80%. The 2% contour thus indicates 4×10^{-4} in the actual trace. (b) The SHG FROG trace computed for the retrieved intensity and phase. Note that details at the level of 4×10^{-4} are reproduced. (c) The retrieved intensity and phase for this trace. Note the satellite pulses at the $\sim 10^{-4}$ level.

field, $E(t)$ or $E(t - \tau)$, is squared in the above expression. The choice is irrelevant and only serves to reflect the trace with respect to τ .

The main advantage of THG FROG is that, like the other third-order FROG methods, it removes the direction-of-time ambiguity that occurs in SHG FROG. In addition, the STHG effect is sufficiently strong that STHG FROG can be used to measure unamplified pulses from a Ti:sapphire oscillator. Indeed, currently, the only third-order FROG method to achieve this measurement has been STHG FROG.

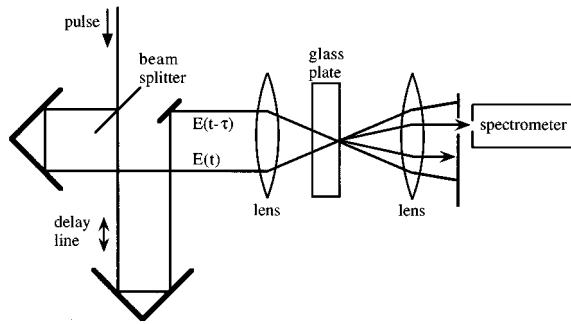


FIG. 10. Experimental apparatus for THG FROG (from Tsang *et al.* Ref. 81). Note that the two pulses overlap spatially at the exit face of the glass medium.

In terms of its performance, THG FROG is intermediate between SHG FROG and the other third-order FROG methods. It is less sensitive than SHG FROG, but more sensitive than PG and SD FROG. Its traces are similar to SHG FROG traces—somewhat unintuitive—but they have a slight asymmetry that distinguishes them from SHG FROG traces and removes the direction-of-time ambiguity. On the other hand, THG FROG traces are not as intuitive as the other third-order FROG traces. And while THG FROG lacks the direction-of-time ambiguity of SHG FROG, it does have relative-phase ambiguities with well-separated multiple pulses, as is the case for SHG FROG, but not for the other third-order FROG methods. And, for pulses that are perfectly linearly chirped and perfectly Gaussian in intensity, the sign of the chirp parameter is indeterminate in THG FROG (although this is extremely unlikely to occur in practice). Thus, THG FROG and its special case, STHG FROG, represent a compromise between other FROG variations and hence may best be used only in special cases, such as for the measurement of an unamplified oscillator pulse train when only one trace can be made, no additional information is available, and direction-of-time ambiguity is unacceptable.

There is a unique advantage to STHG FROG, however, and that is that the THG interaction is a surface effect, so the phase-matching bandwidth is extremely large. As a result, STHG FROG may be ideal for extremely short laser pulses, which require such a thin SHG crystal that SHG FROG measurements are difficult. For example, 10 fs pulses at 800 nm require a KDP crystal with a thickness of about 30 μm or less, which is possible to obtain, but not a trivial polishing task. Thinner crystals represent even greater challenges. Consequently, Ti:sapphire pulses ~ 5 fs in duration may best be measured with STHG FROG. Note that STHG would be preferred for this measurement over surface SHG, because surface SHG is significantly weaker than surface THG.

F. Additional experimental issues

In all FROG measurements, it is essential to measure the entire trace: the trace should be an island in a sea of zeros. That no cropping of the trace should occur may seem an obvious point, but cropped traces are the most common cause for poor retrieval for new users of FROG.

It should also be mentioned that fused silica is not the only material that can be used for third-order FROG measurements of ultrashort laser pulses. Any strongly nonlinear fast-responding material can be used. Luther–Davies *et al.*⁸² have used the thin-film polymer, PPV, which offers excellent signal strength in very thin (few micron) thickness. Heavy-metal-doped glasses also appear promising.

Other nonlinear-optical processes can also be used. We have, for example, recently shown that cascaded second-order processes can mimic the polarization-gate geometry, but with a much stronger effective nonlinearity.⁸³ The application of this idea to FROG will be published soon. Parametric up or down conversion may also be used. Any other fast nonlinear-optical process can produce an autocorrelation measurement, and hence a FROG measurement, as well. It is simply necessary to modify the algorithm to account for the change in the expression for the signal field, as will be discussed in Sec. VII.

VII. THE FROG PULSE RETRIEVAL ALGORITHM

Several FROG pulse-retrieval algorithms^{17,21,25,26,79,84} have been published, and the best possible computer program for pulse retrieval would incorporate all of them, switching from one to another as one stagnates. We have found one exception to this rule, however, and that is that the use of an independently measured spectrum as an additional constraint⁷⁹ tends to cause instabilities due to a required deconvolution and hence is not recommended.¹⁶ In addition, we have found that one algorithmic technique is so reliable and so superior to the others that most pulses can be retrieved with it alone. That algorithmic method is called generalized projections,²⁶ and it is frequently used in phase-retrieval problems unrelated to FROG. It is also commonly used in many other problems, from x-ray crystallography to the training of artificial neural networks. Indeed, it is one of the few algorithmic methods that can be proven to converge when reasonable conditions are met.

The goal of the pulse-retrieval problem in FROG is to find $E(t)$, or, equivalently, $E_{\text{sig}}(t, \tau)$. In order to do this, we observe that there are two equations, or constraints, that $E_{\text{sig}}(t, \tau)$ must satisfy. One is that the measured FROG trace is the squared magnitude of the 1D Fourier transform of $E_{\text{sig}}(t, \tau)$ with respect to time:

$$I_{\text{FROG}}(\omega, \tau) = \left| \int_{-\infty}^{\infty} E_{\text{sig}}(t, \tau) \exp(-i\omega t) dt \right|^2. \quad (14)$$

The other constraint is the mathematical form of the signal field in terms of the pulse field, $E(t)$, for the particular nonlinear-optical process used in the measurement. The various versions of FROG that we have discussed so far have the signal-field forms:

$$E_{\text{sig}}(t, \tau) \propto \begin{cases} E(t)|E(t-\tau)|^2 & \text{for PG FROG} \\ E(t)^2 E^*(t-\tau) & \text{for SD FROG} \\ E(t)E(t-\tau) & \text{for SHG FROG} \\ E(t)^2 E(t-\tau) & \text{for THG FROG} \end{cases}. \quad (15)$$

In this list, we have omitted TG FROG because it yields the same expressions as PG or SD FROG.

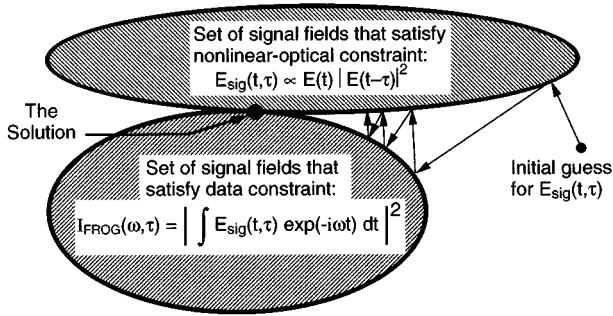


FIG. 11. Geometrical interpretation of the generalized-projections (GP) iterative algorithm, showing that convergence to the correct result (the intersection of the two constraint sets) is guaranteed when the constraint sets are convex. (Convergence remains highly likely even when the sets are not convex, as is the case in FROG.) Figure adapted from article by DeLong *et al.* Ref. 26.

The goal is to find the signal field, $E_{\text{sig}}(t, \tau)$, that satisfies both of these constraints, Eqs. (14) and (15), for the particular beam geometry.

The essence of the generalized projections technique is graphically displayed in Figure 11. Consider Fig. 11 as a Venn diagram in which the entire figure represents the set of all complex functions of two variables, i.e., potential signal fields, $E_{\text{sig}}(t, \tau)$. The signal fields satisfying the data constraint, Eq. (14), are indicated by the upper elliptical region, while those satisfying the mathematical-form constraint, Eq. (15), are indicated by the lower elliptical region. The signal-pulse field satisfying both constraints, the intersection of the two elliptical regions, is the solution. And it uniquely yields the pulse field, $E(t)$.

The solution is found by making “projections,” which have simple geometrical analogs. We begin with an initial guess at an arbitrary point in signal-field space (usually a signal field consisting entirely of random numbers), which typically satisfies neither constraint. We then make a projection onto one of the constraint sets, which consists of moving to the closest point in that set to the initial guess. Call this point the first iteration. From this point, we then project onto the other set, moving to the closest point in that set to the first iteration. This process is continued until the solution is reached. When the two constraint sets are convex (all line segments connecting two points in each constraint set lie entirely within the set), then convergence is guaranteed.

Unfortunately, the constraint sets in FROG are not convex. When a set is not convex, the projection is not necessarily unique, and a “generalized projection” must be defined. The technique is then called generalized projections (GP), and convergence cannot be guaranteed. On the other hand, the error between the FROG trace of the current signal field and the measured FROG trace can be shown to continually decrease with iteration number, and, although it is conceivable that the algorithm may stagnate at a constant value, this approach is quite robust in FROG problems. And, when combined with other algorithmic methods,^{17,25} it is extremely robust.

GP is implemented in FROG by considering the pulse field, $E^{(k)}(t_i)$, the signal field in the $t\tau$ (time delay) domain, $E_{\text{sig}}^{(k)}(t_i, \tau_j)$, and the signal field’s Fourier transform with re-

spect to time, $\tilde{E}_{\text{sig}}^{(k)}(\omega_i, \tau_j)$, where t_i , τ_i , and $\omega_i = 1, \dots, N$. These quantities are each N or N^2 complex numbers. The superscript, (k) , in all of these definitions indicates that these quantities are k^{th} iterations of the actual quantities for the pulse.

In order to perform a GP to the FROG-trace data constraint set, it is simply necessary to replace the magnitude of $\tilde{E}_{\text{sig}}^{(k)}(\omega_i, \tau_j)$ with the square root of the measured FROG trace, $I_{\text{FROG}}(\omega_i, \tau_j)$. It is easy to show that this simple replacement yields the smallest change in the signal field that is consistent with measured trace. Thus, this simple replacement is a GP for all versions of FROG.

It is, however, more difficult to perform a GP to the mathematical-form constraint set. The goal here is to find the closest signal field to the current iteration for the signal field, $E_{\text{sig}}^{(k)}(t_i, \tau_j)$, that has the desired mathematical form [Eq. (15)] for the particular version of FROG. In other words, we wish to find the new signal field, $E_{\text{sig}}^{(k+1)}(t_i, \tau_j)$, that is, the $k+1^{\text{st}}$ iteration, that minimizes the functional distance:

$$Z = \sum_{i,j=1}^N |E_{\text{sig}}^{(k)}(t_i, \tau_j) - E_{\text{sig}}^{(k+1)}(t_i, \tau_j)|^2 \quad (16)$$

and is of the form of Eq. (15). We can guarantee that both of these conditions are met by explicitly substituting Eq. (15) into the above distance function and solving directly for the pulse field. In particular, for SHG FROG, our goal is to find the pulse field, $E^{(k+1)}(t_i)$, $t_i = 1, \dots, N$, that minimizes the functional distance:

$$Z = \sum_{i,j=1}^N |E_{\text{sig}}^{(k)}(t_i, \tau_j) - E^{(k+1)}(t_i)E^{(k+1)}(t_i - \tau_j)|^2. \quad (17)$$

Z is now a function of the N parameters of the next iteration of the pulse field $E^{(k+1)}(t_i)$, $t_i = 1, \dots, N$. The analogous expression for PG FROG is

$$Z = \sum_{i,j=1}^N |E_{\text{sig}}^{(k)}(t_i, \tau_j) - E^{(k+1)}(t_i)|E^{(k+1)}(t_i - \tau_j)|^2. \quad (18)$$

Once $E^{(k+1)}(t_i)$ is found, the corresponding signal field can be computed for this pulse field using Eq. (15) and will be the next iteration for the signal field, $E_{\text{sig}}^{(k+1)}(t_i, \tau_j)$. Clearly, $E_{\text{sig}}^{(k+1)}(t_i, \tau_j)$ satisfies the mathematical-form constraint exactly. And, because it also minimizes Z , the process in which $E_{\text{sig}}^{(k)}(t_i, \tau_j)$ is replaced with $E_{\text{sig}}^{(k+1)}(t_i, \tau_j)$ is a GP.

In order to perform this minimization, we compute the direction of steepest descent: the negative of the gradient of Z with respect to the field $E^{(k+1)}(t_i)$ at the current value for the field, $E^{(k)}(t_i)$. In other words, we must compute the derivative of Z with respect to each time-point in the complex field. This vector consists of the N complex numbers, $-\partial Z / \partial E^{(k+1)}(t_i)$ evaluated at $E^{(k+1)}(t_i) = E^{(k)}(t_i)$. This computation is somewhat tedious, so we have compiled the expressions for gradients for the various forms of FROG in the Appendix.

In practice, we have found that it is not necessary to find the field, $E(t_i)$, that precisely minimizes Z on each iteration. In principle, in a typical minimization procedure, one would find the distance in the direction of the (negative of the)

gradient that minimizes Z , and then would recompute the above gradient for this new field, find the distance along this new gradient that minimizes Z , etc. In fact, it is only necessary to find the above gradient and to perform the one-dimensional minimization along this direction once. While this new field will not be the precise projection (the minimum of Z), it is approximate, and it suffices in FROG pulse retrieval. Indeed, because it is only one step in a larger procedure, later steps make up for this inaccuracy, and, as a result, this approximate procedure results in a significantly faster pulse-retrieval algorithm overall. And, because the multidimensional surface represented by Z becomes paraboloidal near the global minimum represented by the ultimate solution for the pulse, the overall algorithm is extremely accurate. This process usually requires a few seconds to a few minutes on a PC or Macintosh for 64×64 traces, sometimes longer if the pulse is complicated or the computer slower.

The measure of the success of a pulse measurement using FROG is the ‘‘FROG error.’’ It is the rms difference between the measured trace $I_{\text{FROG}}(\omega_i, \tau_j)$ (normalized to have unity peak) and the trace $I_{\text{FROG}}^{(k)}(\omega_i, \tau_j)$ computed from the retrieved pulse field, $E^{(k)}(t_i)$, where k indicates the most recent iteration. It is given by

$$G = \sqrt{\frac{1}{N^2} \sum_{i,j=1}^N |I_{\text{FROG}}(\omega_i, \tau_j) - \alpha I_{\text{FROG}}^{(k)}(\omega_i, \tau_j)|^2}, \quad (19)$$

where α is the real number that minimizes G (required for renormalization). For noise-free data, G should be limited by machine error (typically, we achieve values of $\sim 10^{-7}$). The resulting FROG error for experimental traces should indicate the experimental error. Typical values for FROG errors achieved in experiments with 128×128 arrays using PG FROG are $< 1\%$ and using SHG FROG are $< 0.5\%$ (because there is less noise background in SHG FROG). Errors tend to be lower for larger arrays because, due to the fast Fourier transform relations between the delay and frequency axis ranges and increments, the fractional area of the trace that is nonzero is less in the larger array traces. The general result is $G \sim (TBP/N)^{1/2} \epsilon$, where TBP is the time-bandwidth product of the pulse, ϵ is the error in the trace data points where the trace is nonzero, and $N \times N$ is the array size.²⁵ In this calculation, we have assumed that the noise is multiplicative. For additive noise, the error pervades the entire trace, so $G \sim \epsilon$, independent of TBP and N .

There is additional information on the running of this algorithm in another publication we have written, and the interested reader is referred to that publication.³² A user-friendly version of the FROG algorithm can be purchased from Femtosoft (www.wco.com/~fsoft/).

VIII. THE MEASUREMENT OF WEAK OR COMPLEX PULSES: TADPOLE

All techniques for the measurement of ultrashort laser pulses require the use of a nonlinear-optical medium and hence have limited sensitivity. The most sensitive intensity and phase measurement technique known is SHG FROG, and its sensitivity is on the order of 1 pJ for multishot measurements. Many ultrafast-spectroscopy experiments, how-

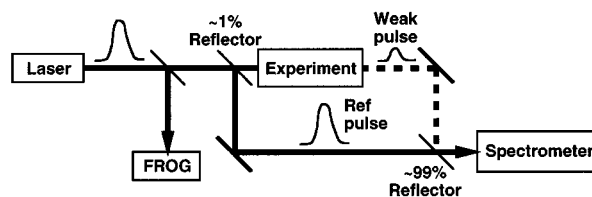


FIG. 12. TADPOLE (the combination of FROG and spectral interferometry) beam geometry (from Fittinghoff *et al.* Ref. 18). Measurement of the spectrum of the sum of two pulses is sufficient to yield the intensity and phase of one of the pulses if the other pulse intensity and phase is known.

ever, produce signal pulses with fJ of energy or less. Of course, the information available in the spectroscopy measurement would be greatly enhanced if full characterization of the ultraweak signal pulse were possible.^{85–87} Thus, it is desirable to be able to measure weaker pulses.

While such a measurement would seem nearly impossible, it can be achieved in nearly all cases by making the following observation: ultraweak pulses never occur alone; they are always created by significantly stronger pulses interacting in some manner with a medium. As a result, the stronger pulse may be measured using FROG and can be utilized as a known reference pulse for the purpose of measuring the ultraweak unknown pulse. A variety of techniques that utilize a reference pulse are available. Probably the simplest and most sensitive is spectral interferometry, which has been known since 1896.^{85,86,88–99}

Spectral interferometry involves simply measuring the spectrum of the sum of a reference pulse and the unknown pulse. This yields sufficient information to fully determine the unknown pulse, provided the reference pulse is known. Since spectral interferometry is an entirely linear measurement, it is extremely sensitive. Fittinghoff *et al.*,¹⁸ (calling the combination of FROG and spectral interferometry: temporal analysis by dispersing a pair of light E-fields or TADPOLE), have measured a reference pulse using SHG FROG and have used this known pulse to measure the full intensity and phase of a train of pulses containing on average 1/5 of a photon each. The beam geometry for this measurement is shown in Fig. 12.

We should also mention that complex shaped pulses are probably best measured with TADPOLE because it requires only a single spectral measurement. FROG, on the other hand, requires N spectral measurements to produce the full $N \times N$ time-frequency-domain trace. Thus, a pulse with significant structure can yield a very large FROG trace and require a long time for algorithm convergence. In addition, complex shaped pulses are usually created using a pulse-shaping apparatus that starts with a very simple smooth pulse. Consequently, the simple pulse could be measured with FROG and then used as the reference pulse for measuring the shaped pulse using spectral interferometry. Such a TADPOLE set up would significantly simplify the measurement and the analysis.

In addition, since spectral interferometry requires measuring only a single spectrum, the remaining rows of the camera array could then be used to obtain intensity and phase information as a function of a spatial coordinate of the

beam. In such a measurement, it is important that the reference pulse is spatially filtered to ensure flat-phase wavefronts (or at least known wavefronts). This has been done with a fully characterized reference pulse¹⁰⁰ and previously with an uncharacterized reference pulse.⁹⁴

In addition, both polarizations may be measured simultaneously using TADPOLE, and, as a result, the time-dependent polarization of a weak ultrashort pulse may be measured. This has been done, and the method has been called polarization labeled interference versus wavelength for only a glint (POLLIWOG).¹⁰¹

While detailed discussion of the work mentioned in this section is beyond the scope of this article, we mention it here for completeness and refer the interested reader to the original articles on this subject.

IX. FUTURE DIRECTIONS

In practice, FROG works well. There are, however, some improvements that will be welcome. The FROG algorithm requires a minute or so to converge, and it would be nice to speed up the process. We are currently developing an artificial neural network for retrieving pulses from FROG traces. The advantage of the use of a neural net is that, while training such a net is very time consuming, running the resulting net on a trace will be very fast. The running of the net is simply a finite set of multiplications and additions, with no iterations involved. The computer time required for such a computation is on the order of milliseconds. Preliminary results for a reduced set of pulses have been encouraging.¹⁰²

Work is underway to extend FROG to other wavelength ranges. Recent efforts have demonstrated FROG at mid-IR wavelengths.^{33,35} These efforts can be considered straightforward because autocorrelations have been demonstrated for many wavelengths. We look forward to seeing such demonstrations in other ranges as well.

Finally, while the combination of FROG and spectral interferometry solves many problems that would be impossible to solve with FROG or spectral interferometry alone, it would be helpful if FROG's sensitivity and range of pulse complexities could be extended, so that the spectral interferometer is not necessary for some applications. Fortunately, materials studies relevant to other problems, such as optical communications and computing, will produce new materials with fast and large nonlinearities and hence will benefit ultrashort-pulse measurement, as well. As a result, we can look forward to rapid advances in ultrashort-pulse measurement as they occur elsewhere.

ACKNOWLEDGMENTS

This work was partially supported by the U.S. Department of Energy, Basic Energy Sciences, Chemical Sciences Division. It was also partially supported by a Department of Energy Cooperative Research And Development Agreement and a Sandia Laboratory-Directed Research and Development grant. M. A. Krumbügel gratefully acknowledges the support of the Alexander von Humboldt Foundation under the Feodor Lynen program. Finally, the authors would like to

thank the Optical Society of America for permission to reprint Figs. 6, 7, 10, 11, and 12 from previous OSA publications.

APPENDIX: EXPRESSIONS FOR THE MATHEMATICAL-FORM-CONSTRAINT GRADIENT FOR IMPLEMENTATION OF GENERALIZED PROJECTIONS IN FROG PULSE RETRIEVAL

In the FROG pulse-retrieval algorithm, it is necessary, when using the generalized-projections technique, to minimize the functional distance, Z , [Eq. (16)]. In order to do this, we compute the gradient of Z with respect to $E^{(k+1)}(t_k)$, where $t_k = 1, \dots, N$. We will thus need to compute $\partial Z / \partial E^{(k+1)}(t_k)$ for each value of t_k . Each of these N complex quantities is then a component of the complex gradient vector. In practice, we actually compute the $2N$ real quantities, $\partial Z / [\text{Re}\{\partial E^{(k+1)}(t_k)\}]$ and $\partial Z / [\text{Im}\{\partial E^{(k+1)}(t_k)\}]$. The expressions for these quantities are given below. Note that, in this Appendix, we have dropped the superscripts to simplify the complex equations that result. This can be done because, throughout this Appendix, the signal field, $E_{\text{sig}}(t, \tau)$, always indicates the k^{th} iteration for the signal field [$E_{\text{sig}}^{(k)}(t_i, \tau_j)$ in the text], and the pulse field, $E(t)$, always indicates the $k+1^{\text{st}}$ iteration for the pulse field ($E^{(k+1)}(t_k)$ in the text). Finally, in these computations, we will make use of the simple results:

$$\begin{aligned} \frac{\partial E(t_i)}{\partial \text{Re}\{E(t_k)\}} &= \delta(t_i - t_k) & \frac{\partial E(t_i)}{\partial \text{Im}\{E(t_k)\}} &= i \delta(t_i - t_k), \\ \frac{\partial E^*(t_i)}{\partial \text{Re}\{E(t_k)\}} &= \delta(t_i - t_k) & \frac{\partial E^*(t_i)}{\partial \text{Im}\{E(t_k)\}} &= -i \delta(t_i - t_k), \\ \frac{\partial E(t_i - \tau_j)}{\partial \text{Re}\{E(t_k)\}} &= \delta(t_i - \tau_j - t_k) & \frac{\partial E(t_i - \tau_j)}{\partial \text{Im}\{E(t_k)\}} &= i \delta(t_i - \tau_j - t_k), \\ \frac{\partial E^*(t_i - \tau_j)}{\partial \text{Re}\{E(t_k)\}} &= \delta(t_i - \tau_j - t_k), & & \\ \frac{\partial E^*(t_i - \tau_j)}{\partial \text{Im}\{E(t_k)\}} &= -i \delta(t_i - \tau_j - t_k). \end{aligned} \quad (\text{A1})$$

A. SHG FROG

We consider SHG FROG first because its equations are the simplest. In SHG FROG, the signal field is given by

$$E_{\text{sig}}^{\text{SHG}}(t, \tau) = E(t)E(t - \tau). \quad (\text{A2})$$

So the distance function to be minimized is

$$Z^{\text{SHG}} = \sum_{i,j=1}^N |E_{\text{sig}}(t_i, \tau_j) - E(t_i)E(t_i - \tau_j)|^2. \quad (\text{A3})$$

The required gradient is then

$$\begin{aligned} \frac{\partial Z^{\text{SHG}}}{\partial \text{Re}\{E(t_k)\}} &= \sum_{i,j=1}^N \left(- \frac{\partial E(t_i)}{\partial \text{Re}\{E(t_k)\}} E(t_i - \tau_j) \right. \\ &\quad \left. - E(t_i) \frac{\partial E(t_i - \tau_j)}{\partial \text{Re}\{E(t_k)\}} \right) \sigma^{\text{SHG}*} + \text{c.c.}, \end{aligned} \quad (\text{A4})$$

where σ^{SHG} is the quantity in the absolute-value brackets in Eq. (A3). Using Eq. (A1), we have

$$= \sum_{i,j=1}^N (-\delta(t_i - t_k)E(t_i - \tau_j) - E(t_i)\delta(t_i - \tau_j - t_k))\sigma^{\text{SHG}*} + \text{c.c.} \quad (\text{A5})$$

Substituting for σ^{SHG}

$$= \sum_{j=1}^N -E_{\text{sig}}^*(t_k, \tau_j)E(t_k - \tau_j) + E^*(t_k)|E(t_k - \tau_j)|^2 - E_{\text{sig}}^*(t_k + \tau_j, \tau_j)E(t_k + \tau_j) + E^*(t_k)|E(t_k + \tau_j)|^2 + \text{c.c.} \quad (\text{A6})$$

Similarly,

$$\frac{\partial Z^{\text{SHG}}}{\partial \text{Im}\{E(t_k)\}} = \sum_{i,j=1}^N \left(-\frac{\partial E(t_i)}{\partial \text{Im}\{E(t_k)\}} E(t_i - \tau_j) - E(t_i) \frac{\partial E(t_i - \tau_j)}{\partial \text{Im}\{E(t_k)\}} \right) \sigma^{\text{SHG}*} + \text{c.c.} \quad (\text{A7})$$

$$= i \sum_{i,j=1}^N (-\delta(t_i - t_k)E(t_i - \tau_j) - E(t_i)\delta(t_i - \tau_j - t_k)) \times \sigma^{\text{SHG}*} + \text{c.c.} \quad (\text{A8})$$

$$= i \sum_{j=1}^N -E_{\text{sig}}^{\prime*}(t_k, \tau_j)E(t_k - \tau_j) + E^*(t_k)|E(t_k - \tau_j)|^2 - E_{\text{sig}}^{\prime*}(t_k + \tau_j, \tau_j)E(t_k + \tau_j) + E^*(t_k)|E(t_k + \tau_j)|^2 + \text{c.c.} \quad (\text{A9})$$

B. PG FROG

In PG FROG, the signal field is given by

$$E_{\text{sig}}^{\text{PG}}(t, \tau) = E(t)|E(t - \tau)|^2. \quad (\text{A10})$$

So the distance function to be minimized is

$$Z^{\text{PG}} = \sum_{i,j=1}^N |E_{\text{sig}}(t_i, \tau_j) - E(t_i)|E(t_i - \tau_j)|^2|^2. \quad (\text{A11})$$

The gradient is then

$$\frac{\partial Z^{\text{PG}}}{\partial \text{Re}\{E(t_k)\}} = \sum_{i,j=1}^N \left(-\frac{\partial E(t_i)}{\partial \text{Re}\{E(t_k)\}} \left| E(t_i - \tau_j) \right|^2 - E(t_i) \frac{\partial E(t_i - \tau_j)}{\partial \text{Re}\{E(t_k)\}} E^*(t_i - \tau_j) - E(t_i)E(t_i - \tau_j) \frac{\partial E^*(t_i - \tau_j)}{\partial \text{Re}\{E(t_k)\}} \right) \sigma^{\text{PG}*} + \text{c.c.}, \quad (\text{A12})$$

where σ^{PG} is the quantity in the outer absolute-value brackets in Eq. (A11). Using Eq. (A1), we have

$$= \sum_{i,j=1}^N (-\delta(t_i - t_k)|E(t_i - \tau_j)|^2 - E(t_i)\delta(t_i - \tau_j - t_k)E^* \times (t_i - \tau_j) - E(t_i)E(t_i - \tau_j)\delta(t_i - \tau_j - t_k))\sigma^{\text{PG}*} + \text{c.c.}, \quad (\text{A13})$$

$$= \sum_{j=1}^N -E_{\text{sig}}^{\prime*}(t_k, \tau_j)|E(t_k - \tau_j)|^2 + E^*(t_k)|E(t_k - \tau_j)|^4 - (E(t_k) + E^*(t_k))(E_{\text{sig}}^{\prime*}(t_k + \tau_j, \tau_j)E(t_k + \tau_j) - |E(t_k)E(t_k + \tau_j)|^2) + \text{c.c.} \quad (\text{A14})$$

$$- (E(t_k) + E^*(t_k))(E_{\text{sig}}^{\prime*}(t_k + \tau_j, \tau_j)E(t_k + \tau_j) - |E(t_k)E(t_k + \tau_j)|^2) + \text{c.c.} \quad (\text{A15})$$

and

$$\frac{\partial Z^{\text{PG}}}{\partial \text{Im}\{E(t_k)\}} = \sum_{i,j=1}^N \left(-\frac{\partial E(t_i)}{\partial \text{Im}\{E(t_k)\}} \left| E(t_i - \tau_j) \right|^2 - E(t_i) \frac{\partial E(t_i - \tau_j)}{\partial \text{Im}\{E(t_k)\}} E^*(t_i - \tau_j) - E(t_i - \tau_j) \frac{\partial E(t_i - \tau_j)}{\partial \text{Im}\{E(t_k)\}} E^*(t_i - \tau_j) \times E(t_i) \frac{\partial E^*(t_i - \tau_j)}{\partial \text{Im}\{E(t_k)\}} \right) \sigma^{\text{PG}*} + \text{c.c.}, \quad (\text{A16})$$

$$= i \sum_{i,j=1}^N (-\delta(t_i - t_k)|E(t_i - \tau_j)|^2 - E(t_i)\delta(t_i - \tau_j - t_k) \times E^*(t_i - \tau_j) + E(t_i)E(t_i - \tau_j)\delta(t_i - \tau_j - t_k))\sigma^{\text{PG}*} + \text{c.c.}, \quad (\text{A17})$$

$$= i \sum_{j=1}^N (-E_{\text{sig}}^{\prime*}(t_k, \tau_j)|E(t_k + \tau_j)|^2 + E^*(t_k)|E(t_k - \tau_j)|^4 - (E^*(t_k) - E(t_k))(E_{\text{sig}}^{\prime*}(t_k + \tau_j, \tau_j)E(t_k + \tau_j) - |E(t_k)E(t_k + \tau_j)|^2)) + \text{c.c.} \quad (\text{A18})$$

C. SD FROG

In SD FROG, the signal field is given by

$$E_{\text{sig}}^{\text{SD}}(t, \tau) = E^2(t)E^*(t - \tau). \quad (\text{A19})$$

So the distance function to be minimized is

$$Z^{\text{SD}} = \sum_{i,j=1}^N |E_{\text{sig}}(t_i, \tau_j) - E^2(t_i)E^*(t_i - \tau_j)|^2 \quad (\text{A20})$$

$$\frac{\partial Z^{\text{SD}}}{\partial \text{Re}\{E(t_k)\}} = \sum_{i,j=1}^N \left(-2E(t_i) \frac{\partial E(t_i)}{\partial \text{Re}\{E(t_k)\}} E^*(t_i - \tau_j) - E^2(t_i) \frac{\partial E^*(t_i - \tau_j)}{\partial \text{Re}\{E(t_k)\}} \right) \sigma^{\text{SD}*} + \text{c.c.}, \quad (\text{A21})$$

where σ^{SD} is the quantity in the absolute-value brackets in Eq. (A20). Using Eq. (A1), we have

$$= \sum_{i,j=1}^N (-2E(t_i)\delta(t_i - t_k)E^*(t_i - \tau_j) - E^2(t_i) \times \delta(t_i - \tau_j - t_k))\sigma^{\text{SD}*} + \text{c.c.} \quad (\text{A22})$$

$$\begin{aligned}
&= \sum_{j=1}^N -2E'_{\text{sig}}{}^*(t_k, \tau_j)E(t_k)E^*(t_k - \tau_j) \\
&\quad + 2E^*(t_k)|E(t_k)E(t_k - \tau_j)|^2 - E'_{\text{sig}}{}^*(t_k + \tau_j, \tau_j) \\
&\quad \times E^2(t_k + \tau_j) + E(t_k)|E(t_k + \tau_j)|^4 + \text{c.c.} \quad (\text{A23})
\end{aligned}$$

and

$$\begin{aligned}
\frac{\partial Z^{\text{SD}}}{\partial \text{Im}\{E(t_k)\}} &= \sum_{i,j=1}^N \left(-2E(t_i) \frac{\partial E(t_i)}{\partial \text{Im}\{E(t_k)\}} E^*(t_i - \tau_j) \right. \\
&\quad \left. - E^2(t_i) \frac{\partial E^*(t_i - \tau_j)}{\partial \text{Im}\{E(t_k)\}} \right) \sigma^{\text{SD}*} + \text{c.c.} \quad (\text{A24})
\end{aligned}$$

$$\begin{aligned}
&= i \sum_{i,j=1}^N (-2E(t_i) \delta(t_i - t_k) E^*(t_i - \tau_j) + E^2(t_i) \\
&\quad \times \delta(t_i - \tau_j - t_k)) \sigma^{\text{SD}*} + \text{c.c.} \quad (\text{A25})
\end{aligned}$$

$$\begin{aligned}
&= i \sum_{j=1}^N -2E'_{\text{sig}}{}^*(t_k, \tau_j)E(t_k)E^*(t_k - \tau_j) \\
&\quad + 2E^*(t_k)|E(t_k)E(t_k - \tau_j)|^2 + E'_{\text{sig}}{}^*(t_k + \tau_j, \tau_j) \\
&\quad \times E^2(t_k + \tau_j) - E(t_k)|E(t_k + \tau_j)|^4 + \text{c.c.} \quad (\text{A26})
\end{aligned}$$

D. THG FROG

In THG FROG, the signal field is given by

$$E_{\text{sig}}^{\text{THG}}(t, \tau) = E^2(t)E(t - \tau). \quad (\text{A27})$$

So the distance function to be minimized is

$$Z^{\text{THG}} = \sum_{i,j=1}^N |E_{\text{sig}}(t_i, \tau_j) - E^2(t_i)E(t_i - \tau_j)|^2. \quad (\text{A28})$$

The gradient is then

$$\begin{aligned}
\frac{\partial Z^{\text{THG}}}{\partial \text{Re}\{E(t_k)\}} &= \sum_{i,j=1}^N \left(-2E(t_i) \frac{\partial E(t_i)}{\partial \text{Re}\{E(t_k)\}} E(t_i - \tau_j) \right. \\
&\quad \left. - E^2(t_i) \frac{\partial E(t_i - \tau_j)}{\partial \text{Re}\{E(t_k)\}} \right) \sigma^{\text{THG}*} + \text{c.c.}, \quad (\text{A29})
\end{aligned}$$

where σ^{THG} is the quantity in the absolute-value brackets in Eq. (A28). Using Eq. (A1), we have

$$\begin{aligned}
&= \sum_{i,j=1}^N (-2E(t_i) \delta(t_i - t_k) E(t_i - \tau_j) - E^2(t_i) \\
&\quad \times \delta(t_i - \tau_j - t_k)) \sigma^{\text{THG}*} + \text{c.c.} \quad (\text{A30}) \\
&= \sum_{j=1}^N -2E'_{\text{sig}}{}^*(t_k, \tau_j)E(t_k)E(t_k - \tau_j) + 2E^*(t_k) \\
&\quad \times |E(t_k)E(t_k - \tau_j)|^2 \\
&\quad - E'_{\text{sig}}{}^*(t_k + \tau_j, \tau_j)E^2(t_k + \tau_j) \\
&\quad + E^*(t_k)|E(t_k + \tau_j)|^4 + \text{c.c.} \quad (\text{A31})
\end{aligned}$$

and

$$\begin{aligned}
\frac{\partial Z^{\text{THG}}}{\partial \text{Im}\{E(t_k)\}} &= \sum_{i,j=1}^N \left(-2E(t_i) \frac{\partial E(t_i)}{\partial \text{Im}\{E(t_k)\}} E(t_i - \tau_j) \right. \\
&\quad \left. - E^2(t_i) \frac{\partial E(t_i - \tau_j)}{\partial \text{Im}\{E(t_k)\}} \right) \sigma^{\text{THG}*} + \text{c.c.} \quad (\text{A32})
\end{aligned}$$

$$\begin{aligned}
&= i \sum_{i,j=1}^N (-2E(t_i) \delta(t_i - t_k) E(t_i - \tau_j) - E^2(t_i) \\
&\quad \times \delta(t_i - \tau_j - t_k)) \sigma^{\text{THG}*} + \text{c.c.} \quad (\text{A33})
\end{aligned}$$

$$\begin{aligned}
&= i \sum_{j=1}^N -2E'_{\text{sig}}{}^*(t_k, \tau_j)E(t_k)E(t_k - \tau_j) \\
&\quad + 2E^*(t_k)|E(t_k)E(t_k - \tau_j)|^2 - E'_{\text{sig}}{}^*(t_k + \tau_j, \tau_j) \\
&\quad \times E^2(t_k + \tau_j) + E^*(t_k)|E(t_k + \tau_j)|^4 + \text{c.c.} \quad (\text{A34})
\end{aligned}$$

¹J. Zhou, G. Taft, C. P. Huang, M. M. Murnane, H. C. Kapteyn, and I. Christov, *Opt. Lett.* **19**, 1149 (1994).

²L. Xu, D. Spielmann, F. Krausz, and R. Szipocs, *Opt. Lett.* **21**, 1259 (1996).

³I. P. Christov, V. Stoev, M. M. Murnane, and H. C. Kapteyn, *Opt. Lett.* **21**, 1493 (1996).

⁴M. Nisoli, S. D. Silvestri, and O. Svelto, *Opt. Lett.* **68**, 2793 (1996).

⁵G. J. Tearney, B. E. Bouma, S. A. Boppart, B. Golubovic, E. A. Swanson, and J. G. Fujimoto, *Opt. Lett.* **21**, 1408 (1996).

⁶B. Kohler, V. V. Yakovlev, J. Che, J. L. Krause, M. Messina, K. R. Wilson, N. Schwentner, R. M. Whittell, and Y. Yan, *Phys. Rev. Lett.* **74**, 3360 (1995).

⁷H. L. Fragnito, J.-Y. Bigot, P. C. Becker, and C. V. Shank, *Chin. Phys. Lasers* **160**, 101 (1989).

⁸K. Svoboda, W. Denk, W. H. Knox, and T. Tsuda, *Opt. Lett.* **21**, 1411 (1996).

⁹I. P. Christov, M. M. Murnane, H. C. Kapteyn, J. P. Zhou, and C. P. Huang, *Opt. Lett.* **19**, 1465 (1994).

¹⁰J. D. Harvey, J. M. Dudley, P. F. Curley, C. Spielmann, and F. Krausz, *Opt. Lett.* **19**, 972 (1994).

¹¹P. Zhou, H. Schulz, and P. Kohns, *Opt. Commun.* **123**, 501 (1996).

¹²T. S. Clement, G. Rodriguez, W. M. Wood, and A. J. Taylor, *Proc. SPIE* **2701**, 229 (1996).

¹³M. Dugan, J. X. Tull, J.-K. Rhee, and W. S. Warren, in *Ultrafast Phenomena X*, Vol. 62, edited by P. F. Barbara, J. G. Fujimoto, W. H. Knox, and W. Zinth (Springer, Berlin, 1996), pp. 26 and 27.

¹⁴A. M. Weiner, *Progress in Quantum Electronics*, 1995 (unpublished).

¹⁵J. L. A. Chilla and O. E. Martinez, *Opt. Lett.* **16**, 39 (1991).

¹⁶K. W. DeLong, R. Trebino, J. Hunter, and W. E. White, *J. Opt. Soc. Am. B* **11**, 2206 (1994).

¹⁷R. Trebino and D. J. Kane, *J. Opt. Soc. Am. A* **10**, 1101 (1993).

¹⁸D. N. Fittinghoff, J. L. Bowie, J. N. Sweetser, R. T. Jennings, M. A. Krumbügel, K. W. DeLong, R. Trebino, and I. A. Walmsley, *Opt. Lett.* **21**, 884 (1996).

¹⁹K. C. Chu, J. P. Heritage, R. Grant, K. Liu, A. Dienes, W. E. White, and A. Sullivan, *Opt. Lett.* **20**, 904 (1995).

²⁰B. S. Prade, J. M. Schins, E. T. J. Nibbering, M. A. Franco, and A. Mysyrowickz, *Opt. Commun.* **113**, 79 (1995).

²¹D. J. Kane and R. Trebino, *Opt. Lett.* **18**, 823 (1993).

²²D. J. Kane and R. Trebino, *IEEE J. Quantum Electron.* **29**, 571 (1993).

²³K. W. DeLong, R. Trebino, and D. J. Kane, *J. Opt. Soc. Am. B* **11**, 1595 (1994).

²⁴D. J. Kane, A. J. Taylor, R. Trebino, and K. W. DeLong, *Opt. Lett.* **19**, 1061 (1994).

²⁵K. W. DeLong and R. Trebino, *J. Opt. Soc. Am. A* **11**, 2429 (1994).

²⁶K. W. DeLong, D. N. Fittinghoff, R. Trebino, B. Kohler, and K. Wilson, *Opt. Lett.* **19**, 2152 (1994).

²⁷K. W. DeLong, R. Trebino, and W. E. White, *J. Opt. Soc. Am. B* **12**, 2463 (1995).

²⁸D. N. Fittinghoff, K. W. DeLong, R. Trebino, and C. L. Ladera, *J. Opt. Soc. Am. B* **12**, 1955 (1995).

- ²⁹G. Taft, A. Rundquist, M. M. Murnane, H. C. Kapteyn, K. W. DeLong, R. Trebino, and I. P. Christov, *Opt. Lett.* **20**, 743 (1995).
- ³⁰K. W. DeLong, R. Trebino, D. N. Fittinghoff, and C. L. Ladera, in *Generation, Amplification, and Measurement of Ultrashort Laser Pulses II*, Vol. 2377, edited by F. W. Wise and C. P. J. Barty (Society of Photo-Optical Instrumentation Engineers, Bellingham, 1995), pp. 44–51.
- ³¹T. S. Clement, A. J. Taylor, and D. J. Kane, *Opt. Lett.* **20**, 70 (1995).
- ³²K. W. DeLong, D. N. Fittinghoff, and R. Trebino, *IEEE J. Quantum Electron.* **32**, 1253 (1996).
- ³³B. A. Richman, M. A. Krumbügel, and R. Trebino, in *Generation, Amplification, and Measurement of Ultrashort Laser Pulses III*, Vol. 2701, edited by W. E. White and D. H. Reitze (Society of Photo-Optical Instrumentation Engineers, Bellingham, 1996).
- ³⁴G. Taft, M. Rundquist, I. P. Christov, H. C. Kapteyn, K. W. DeLong, D. N. Fittinghoff, M. A. Krumbügel, J. N. Sweetser, and R. Trebino, *Selected Topics in Quant. Electron.*, Vol. 2 no. 3, Special Issue on Ultrafast Phenomena, 1997 (unpublished).
- ³⁵B. A. Richman, K. W. DeLong, and R. Trebino, *Nucl. Instrum. Methods Phys. Res. A* **358**, 268 (1995).
- ³⁶M. Maier, W. Kaiser, and J. A. Giordmaine, *Phys. Rev. Lett.* **17**, 1275 (1966).
- ³⁷J. A. Giordmaine, P. M. Rentzepis, S. L. Shapiro, and K. W. Wecht, *Appl. Phys. Lett.* **11**, 216 (1967).
- ³⁸E. P. Ippen and C. V. Shank, *Ultrashort Light Pulses-Picosecond Techniques and Applications* (Springer, Berlin, 1977).
- ³⁹J. C. Diels, J. J. Fontaine, and F. Simoni, in *Proceedings of the International Conference on Lasers* (STS McLean, VA, 1983), pp. 348–355.
- ⁴⁰J. C. M. Diels, J. J. Fontaine, I. C. McMichael, and F. Simoni, *Appl. Opt.* **24**, 1270 (1985).
- ⁴¹J. C. Diels, in *Ultrashort Pulse Spectroscopy and Applications, Proceedings of SPIE*, Vol. 533 (SPIE, Bellingham, 1985), pp. 63–70.
- ⁴²J. C. M. Diels, J. J. Fontaine, N. Jamasbi, and M. Lai, presented at Conference on Lasers & Electro-Optics, 1987 (unpublished).
- ⁴³R. Trebino, C. C. Hayden, A. M. Johnson, W. M. Simpson, and A. M. Levine, *Opt. Lett.* **15**, 1079 (1990).
- ⁴⁴K. Naganuma, K. Mogi, and H. Yamada, *IEEE J. Quantum Electron.* **25**, 1225 (1989).
- ⁴⁵J. Janszky and G. Corradi, *Opt. Commun.* **60**, 251 (1986).
- ⁴⁶A. S. L. Gomes, V. L. da Silva, and J. R. Taylor, *J. Opt. Soc. Am. B* **5**, 373 (1988).
- ⁴⁷J. E. Rothenberg and D. Grischkowski, *Opt. Lett.* **12**, 99 (1987).
- ⁴⁸I. A. Walmsley and R. Trebino, *Opt. Photonics News* **7**, 23 (1996).
- ⁴⁹R. A. Altes, *J. Acoust. Soc. Am.* **67**, 1232 (1980).
- ⁵⁰L. Cohen, *Proc. IEEE* **77**, 941 (1989).
- ⁵¹S. H. Nawab, T. F. Quatieri, and J. S. Lim, *IEEE Trans. Acoust. Speech Signal Process.* **ASSP-31**, 986 (1983).
- ⁵²D. J. Kane and R. Trebino, in *Ultrafast Phenomena VIII*, edited by J. L. Martin, R. Migus, G. A. Mourou, and A. H. Zewail (Springer, Berlin, 1993).
- ⁵³J. P. Foing, J. P. Likforman, M. Joffre, and A. Migus, *IEEE J. Quantum Electron.* **28**, 2285 (1992).
- ⁵⁴M. Vampouille, A. Barthélémy, B. Colombeau, and C. Froely, *J. Opt.* **15**, 385 (1984).
- ⁵⁵J. L. A. Chilla and O. E. Martinez, *IEEE J. Quantum Electron.* **27**, 1228 (1991).
- ⁵⁶J. L. A. Chilla and O. E. Martinez, *Opt. Commun.* **89**, 434 (1992).
- ⁵⁷J. K. Rhee, T. S. Sosnowski, A. C. Tien, and T. B. Norris, *J. Opt. Soc. Am. B* **13**, 1780 (1996).
- ⁵⁸H. Stark, *Image Recovery: Theory and Application* (Academic, Orlando, 1987).
- ⁵⁹V. V. Kotlyar, P. G. Seraphimovich, and V. A. Soifer, *Optik (Stuttgart)* **94**, 96 (1993).
- ⁶⁰J. R. Fienup, *Appl. Opt.* **21**, 2758 (1982).
- ⁶¹D. Peri, *Appl. Opt.* **26**, 1782 (1987).
- ⁶²E. J. Akutowicz, *Trans. Am. Math. Soc.* **83**, 179 (1956).
- ⁶³E. J. Akutowicz, *Trans. Am. Math. Soc.* **84**, 234 (1957).
- ⁶⁴R. P. Millane, *J. Opt. Soc. Am. A* **7**, 394 (1990).
- ⁶⁵E. B. Treacy, *J. Appl. Phys.* **42**, 3848 (1971).
- ⁶⁶Y. Ishida, K. Naganuma, and T. Yajima, *IEEE J. Quantum Electron.* **21**, 69 (1985).
- ⁶⁷A. Watanabe, S. Tanaka, H. Kobayashi, Y. Ishida, and T. Yajima, *Rev. Sci. Instrum.* **56**, 2259 (1985).
- ⁶⁸A. Watanabe, H. Saito, Y. Ishida, and T. Yajima, *Opt. Commun.* **63**, 320 (1987).
- ⁶⁹K. W. DeLong, C. L. Ladera, R. Trebino, B. Kohler, and K. R. Wilson, *Opt. Lett.* **20**, 486 (1995).
- ⁷⁰B. Kohler, V. V. Yakovlev, K. R. Wilson, J. Squier, K. W. DeLong, and R. Trebino, *Opt. Lett.* **20**, 483 (1994).
- ⁷¹A. C. Tien, S. Kane, J. Squier, B. Kohler, and K. Wilson, *J. Opt. Soc. Am. B* **13**, 1160 (1996).
- ⁷²J. N. Sweetser, D. N. Fittinghoff, and R. Trebino, *Opt. Lett.* **22**, 519 (1997).
- ⁷³H. J. Eichler, U. Klein, and D. Langhans, *Appl. Phys.* **21**, 215 (1980).
- ⁷⁴H. J. Eichler, P. Günter, and D. W. Pohl, *Laser-Induced Dynamic Gratings* (Springer, Berlin, 1986).
- ⁷⁵D. W. Phillion, D. J. Kuizenga, and A. E. Siegman, *Appl. Phys. Lett.* **27**, 85 (1975).
- ⁷⁶A. C. Eckbreth, *Appl. Phys. Lett.* **32**, 421 (1978).
- ⁷⁷R. Trebino, C. E. Barker, and A. E. Siegman, *IEEE J. Quantum Electron.* **QE-22**, 1413 (1986).
- ⁷⁸R. Trebino and A. E. Siegman, *J. Chem. Phys.* **79**, 3621 (1983).
- ⁷⁹J. Paye, M. Ramaswamy, J. G. Fujimoto, and E. P. Ippen, *Opt. Lett.* **18**, 1946 (1993).
- ⁸⁰J. M. Dudley, L. P. Barry, P. G. Bollond, J. D. Harvey, R. Leonhardt, and P. D. Drummond, *Opt. Lett.* **22**, 457 (1997).
- ⁸¹T. Tsang, M. A. Krumbügel, K. W. DeLong, D. N. Fittinghoff, and R. Trebino, *Opt. Lett.* **21**, 1381 (1996).
- ⁸²B. Luther-Davies, M. Samoc, J. Swiatkiewicz, A. Samoc, M. Woodruff, R. Trebino, and K. W. DeLong, *Opt. Commun.* **131**, 301 (1996).
- ⁸³M. A. Krumbügel, J. N. Sweetser, D. N. Fittinghoff, K. W. DeLong, and R. Trebino, *Opt. Lett.* **22**, 245 (1997).
- ⁸⁴D. J. Kane, G. Rodriguez, A. J. Taylor, and T. S. Clement, *J. Opt. Soc. Am. B* (in press).
- ⁸⁵J.-Y. Bigot, M.-A. Mycek, S. Weiss, R. G. Ulbrich, and D. S. Chemla, *Phys. Rev. Lett.* **70**, 3307 (1993).
- ⁸⁶D. S. Chemla, J.-Y. Bigot, M.-A. Mycek, S. Weiss, and W. Schäfer, *Phys. Rev. B* **50**, 8439 (1994).
- ⁸⁷S. Patkar, A. E. Paul, W. Sha, J. A. Bolger, and A. L. Smirl, *Phys. Rev. B* **51**, 10 789 (1995).
- ⁸⁸L. Rayleigh, *Proc. R. Soc. London* **59**, 198 (1896).
- ⁸⁹C. Froehly, A. Lacourt, and J. C. Vienot, *J. Opt. (Paris)* **4**, 183 (1973).
- ⁹⁰J. Piasecki, B. Colombeau, M. Vampouille, C. Froehly, and J. A. Arnaud, *Appl. Opt.* **19**, 3749 (1980).
- ⁹¹F. Reynaud, F. Salin, and A. Barthelemy, *Opt. Lett.* **14**, 275 (1989).
- ⁹²K. Minoshima, M. Taiji, and T. Kobayashi, *Opt. Lett.* **16**, 1683 (1991).
- ⁹³E. Tokunaga, A. Terasaki, and T. Kobayashi, *Opt. Lett.* **17**, 1131 (1992).
- ⁹⁴J. P. Geindre, P. Audebert, A. Rousse, F. Falliès, J. C. Gauthier, A. Mysyrowicz, A. Dos Santos, G. Hamoniaux, and A. Antonetti, *Opt. Lett.* **19**, 1997 (1994).
- ⁹⁵L. Lepetit, G. Cheriaux, and M. Joffre, *J. Opt. Soc. Am. B* **12**, 2467 (1995).
- ⁹⁶K. Misawa and T. Kobayashi, *Opt. Lett.* **20**, 1550 (1995).
- ⁹⁷E. Tokunaga, A. Terasaki, and T. Kobayashi, *J. Opt. Soc. Am. B* **12**, 753 (1995).
- ⁹⁸C. W. Siders, S. P. LeBlanc, D. Fisher, T. Tajima, and M. C. Downer, *Phys. Rev. Lett.* **76**, 3570 (1996).
- ⁹⁹C. W. Siders, S. P. LeBlanc, A. Babine, A. Stepanov, A. Sergeev, T. Tajima, and M. C. Downer, *IEEE Trans. Plasma Sci.* **24**, 301 (1996).
- ¹⁰⁰D. N. Fittinghoff, J. Bowie, J. N. Sweetser, R. T. Jennings, M. A. Krumbügel, K. W. DeLong, R. Trebino, and I. A. Walmsley, in *Generation, Amplification, and Measurement of Ultrashort Laser Pulses III*, edited by W. E. White (Society of Photo-Optical Instrumentation Engineers, Bellingham, 1996).
- ¹⁰¹W. J. Walecki, D. N. Fittinghoff, A. L. Smirl, and R. Trebino, *Opt. Lett.* **22**, 81 (1996).
- ¹⁰²M. A. Krumbügel, C. L. Ladera, K. W. DeLong, D. N. Fittinghoff, J. N. Sweetser, and R. Trebino, *Opt. Lett.* **21**, 143 (1996).